An-Najah National University

Faculty of Graduate Studies

PHOTOCATALYTIC DEGRADATION OF XYLENOL ORANGE DYE BY MAGNETIC FE_3O_4.TIO_2 NANOPARTICLES USING LIGHT EMITTING DIODE (LED)

By

Nadeen Yousef Ahmad Abbas

Supervisors

Dr. Ismail Badran
Dr. Rawan Khalaf

This Thesis is Submitted in Partial Fulfillment of the Requirements for the Degree of Master of Chemistry, Faculty of Graduate Studies, An-Najah National University, Nablus - Palestine.

2024

PHOTOCATALYTIC DEGRADATION OF XYLENOL ORANGE DYE BY MAGNETIC $FE_3O_4.TIO_2$ NANOPARTICLES USING LIGHT EMITTING DIODE (LED)

By

Nadeen Yousef Ahmad Abbas

This Thesis was Defended Successfully on 29/10/2024 and approved by

Dr. Ismail Badran	
Supervisor	Signature
Dr. Rawan Khalaf	
Co-Supervisor	Signature
Dr. Orwa Houshia	
External Examiner	Signature
Dr. Ahed Zyoud	
Internal Examiner	Signature

Dedication

To my dearest parents, whose constant support has been my foundation,
To my beloved sister Nisreen, my second mom, whose love and encouragement have guided me, and to all who believed in me and sparked my passion.
Your enduring faith and limitless love have been my greatest inspiration.
And to myself, for finding the strength to face every challenge and the courage to follow my dreams.

Acknowledgements

First and foremost, I offer my deepest gratitude to Allah, the Most Merciful and Compassionate, for His boundless guidance and blessings throughout this journey. His support has been my source of strength.

To my family, your steadfast support, patience, and sacrifices have been immeasurable. Your love and encouragement have been the core of my perseverance and success.

I would like to extend my sincere gratitude to my primary supervisor, Dr. Ismail Badran, whose exceptional guidance and unwavering support have been essential throughout my research. Your insightful feedback, and constant encouragement have not only shaped this work but have also greatly contributed to my academic and personal growth. I deeply appreciate his dedication and the positive influence he has had on my academic progress. It has been an honor to be your student.

I also extend my thanks to Dr. Rawan Khalaf for her role as co-supervisor. Her involvement in the supervisory process is acknowledged and appreciated.

I would like to thank the Middle East Desalination Research Center (MEDRC) for their generous financial support.

I extend my sincere thanks to my colleagues, Ms. Sahar Salman and Ms. Yasmeen Hamdan, for their invaluable collaboration and encouragement throughout this research.

And to Mr. Ameed Amireh, the lab technician, your technical expertise and assistance have been vital to the success of my research.

Thank you all for your significant contributions and for being an essential part of this journey. Your support and encouragement have meant more than words can express.

Declaration

I, the undersigned, declare that I submitted the thesis entitled:

PHOTOCATALYTIC DEGRADATION OF XYLENOL ORANGE DYE BY MAGNETIC FE_3O_4.TIO_2 NANOPARTICLES USING LIGHT EMITTING DIODE (LED)

I declare that the work provided in this thesis, unless otherwise referenced, is the researcher's own work, and has not been submitted elsewhere for any other degree or qualification.

Student's Name: **Nadeen Yousef Ahmad Abbas**

Signature: 

Date: **29/10/2024**

Table of Contents

List of Tables

List of Figures

List of Appendices

PHOTOCATALYTIC DEGRADATION OF XYLENOL ORANGE DYE BY MAGNETIC $FE_3O_4.TIO_2$ NANOPARTICLES USING LIGHT EMITTING DIODE (LED)

By
Nadeen Yousef Ahmad Abbas
Supervisors
Dr. Ismail Badran
Dr. Rawan Khalaf

Abstract

The aim of this study is to develop a new effective and economical photocatalysis method to purify water from organic dyes under visible light radiation. This is achieved by synthesizing a new photocatalyst that has a small band gap; to make it active under light emitting diode (LED) radiation, and it has magnetic properties that simplify purification of the catalyst post treatment. In this study, the magnetic nano particles of $10\%TiO_2/Fe_3O_4$ were synthesized under basic conditions. The point of zero charge (PZC) of the synthesized photocatalyst was found to equal 4.69. Magnetic nano particles were used as a photocatalyst to purify water from Xylenol Orange Sodium Salt organic dye under LED radiation.

The photocatalytic properties of the synthesized catalyst were analyzed across various parameters, and by referring to the change in the UV-Vis spectrum of the solutions. It was noticed that the synthesized nano particles have the same photocatalytic effect of rutile TiO_2, but they are easier to purify post treatment. Different parameters affecting the photocatalysis were studied such as time, pH of the medium, concentration of Xylenol Orange, amount used of the catalyst, and H_2O_2. It was observed that the photocatalytic efficiency is unaffected by the concentration of the Xylenol Orange solution but decreases as the amount of $10\%TiO_2/Fe_3O_4$ increases. Also, photocatalysis was found to favor acidic conditions with pH ~ 3, and favor presence of H_2O_2. A kinetic study was conducted, it was found that the degradation increases with time, and the rate of the reaction follows the second order rate. The possibility of catalyst's recovery after treatment was examined using several washing solutions. Ethanol was found to be the optimal solution to recover the nano particles post treatment. Also, it was found that the nano particles preserved both magnetic and photocatalytic properties. It was confirmed that the photocatalyst could be used at least in four cycles of photocatalysis. In

conclusion, the synthesized magnetic nano particles of 10%TiO_2/Fe_3O_4 could be used efficiently as a photocatalyst under LED radiation to degrade organic pollutants while being both economically and environmentally friendly.

Keywords: Photocatalysis; photodegradation; light emitting diode (LED); dye; Xylenol Orange; nano particles; PZC; TiO_2; magnetic; Fe_3O_4; H_2O_2; UV-Vis; spectrum.

Chapter One
Introduction

1.1 Background

Water is the cronestone of our universe. Hence, scientists have established a theory called “Follow the water”, which means only wherever water exists life is possible (1). The problem is that 97.5% of water worldwide is present in the form of saline (2, 3). Moreover, 75% of fresh water is present in the form of ice, which makes it unavailable to use (2). Meanwhile, the main source for fresh water is lakes, rivers, and soils (2, 3). Due to the rapid growth of human population, economic activities, climate change and other factors, the water crisis started to be dominant and worrying (2-4). The water crisis is considered as one of the leading problems in the 21st century (2-5). As UNESCO declared in 2021, more than 800,000 die per year due to illness related to drinking unsafe water (4). Furthermore, it was reported that poor water quality causes around 80% of the illness around the world (4).

The water crisis is even worse in Palestine (5-7). Groundwater is the main source for water in Palestine (5, 6). Regardless of its limited quantities, water is in great danger of being unsafe to drink due to pollution (5). The main source of this pollution is contamination with the sewage. Lacking a serious waste management strategy, the rapid growth of number of newly established factories, the uncontrolled individual activities, and the absence of wastewater investment and advanced treatment equipment make it harder to prevent sewage water from leaking into the groundwater (5-7). It was reported that by 2013, only 10% of wastewater was being treated (5). Furthermore, it was noticed that there is no real quality control on water sources in Palestine, which may result polluted water to be consumed unsafely by humans without being noticed (6, 7).

Water pollution could be defined as any physical or chemical change in the natural composition and conditions of water (5). This change could be in the form of a change in the pH, color, smell, or taste of water (8, 9). This change could be due to the presence of dissolved solids, plant waste, nitrate compounds from both humans and animals, industrial waste, heavy metals, dyes, inorganic substances or sewage(5, 8). Such changes will cause a drop in water quality which may make water unsafe to use or to drink.

In most cases, the simple methods of water purification are not sufficient. Water treatment methods like boiling, chlorination, and filtration will not be able to get rid of heavy pollutants like metals, dyes, polymers and other organic and inorganic compounds. Hence, more advanced treatments such as ozonation, UV ray, reverse osmosis, membrane process, nano filtration, microfiltration are needed (9). Meanwhile, most efficient purification are both time consuming and expensive (8). Therefore, new efficient, economical, simple, and fast treatment methods are needed.

1.2 Water Pollutants

Water pollution is an extreme worldwide problem. Urbanization, civilization, rapid increase of human population, and technological growth are affecting water pollution severely and make it more rapid (10). Pesticides, oil leaking, excess use of detergents, industrial chemical leaking, dyes, heavy metals, industrial effluents, leaking from agricultural fields, urban waste, food processing waste, dyes, organic matter from dead animals and plants, and organic volatile compounds are examples of the most famous worldwide water pollutants (8, 10, 11). Increasing the concentration of the previously mentioned pollutants decreases the water quality, or makes it unsafe to consume (10). Some colored organic contamination like dyes, could be easily detected with naked eyes, by detecting change in color of water, especially in the cases of excess contamination (12). Other contaminants are hard to detect. Hence, further analysis techniques are needed.

1.2.1 Dyes

Up until the mid-nineteenth century, all dyes in use were natural, sourced from plants, minerals, and animals (13-15). The number of new recognized dyes was increasing with modernization and social development. Dyes were used in both the textile industry and in the art of painting. Besides, some dyes had symbolic meanings such as purple which is used as show of royalty; because it was hard and rare to be found in nature (13). Color ranges were limited to the basic colors such as red, blue, yellow and green. Dyes were limited in both quantities and color range until Graebe and Liebermann were able to define the unsaturated organic structures of dyes. Then, Witt tried to explain the structure of dyes, but he was not able to figure out the exact structure due to limits of organic chemistry back then (16). Hence, organic chemistry and dyes were developing together.

Dyes are unsaturated organic colorant compounds that absorb specific wavelengths of light, which influence their colors. Each dye has a specific absorption wavelength within the visible region, 400 nm to 700 nm, where it absorbs the most (13, 14, 16). Each wavelength represents a specific color. According to color theory, the reflected observed light is the opposite to the one absorbed. For example, a dye which absorbs all the blue lights will appear in yellow, since yellow and blue are complementary to each other in the color wheel (14, 17). The wavelength of maximum absorption and the corresponding observed color of dyes are determined by their components: chromogen, chromophores, and auxochrome (14-16) .

The first building block of dyes is called chromogen. Chromogens are chemically charged compounds that need to be neutralized by other dye components. If they were not neutralized, they would form an ionic or acidic dyes in the case of negative charge, and a basic or cationic dye in the case of positive charge. Chromogens could be slightly colored in themselves. Indeed, other substituents are needed to give the dye its color. Indeed, the chromogen is not sufficient to give the bright and fixed color of the dye (14-16).

The second component of dyes are called chromophores. Chromophores are unsaturated conjugated organic systems consisting mainly of double bonds. Each chromophore must contain at least one methine group. Mostly, each dye will have an aromatic part and contain either a benzene ring or quinone. Moreover, functional groups such as azo, nitro, nitroso, alkene, thiocarbonyl, carbonyl, sulfur bridge, oxygen bridge are common components of chromophores. The excitations associated with the electrons of such systems will be responsible for the absorptions in the UV-Vis region. Hence, dyes are colored due to the chromophores they contain. Indeed, not all chromophores absorb in the visible region, but they cannot make the dye colored by themselves, hence, a third component may be needed (14-16, 18, 19).

The third component which most dyes have is called auxochrome. Auxochromes are basic functional groups that are colorless, and their absorption is limited to the UV region only. Functionals as carboxylic groups, hydroxyl groups, amino groups, and sulfonic acid groups may work as auxochromes (14, 16). As well, some auxochromes as sulfonic acid group may enhance water solubility of the dye (13). Auxochromes work as color helpers that increase the stability and intensity of the color by shifting the

wavelength of maximum absorption of the dye into the visible region (16). The conjugated systems representing the chromophores in themselves may be colorless and occur in the near visible region. Hence adding auxochromes' substituent will shift the maximum absorption of chromophores to0ward the visible region. In addition, if the chromophore has a light or fainted color, the auxochrome substituent will increase the intensity of that color. Overall, auxochromes will increase the conjugation of the system due to the resonance that will be forming, which will enhance the color of the dye (14-16, 18, 19).

One common classification of dyes is by sorting them to natural and synthetic dyes based on the source they were extracted from (19, 20). Natural dyes are extracted from animals, minerals, and plants. Almost all plants contain dyes within their structure, but not all dyes could be extracted nor could be used commercially in the industrial field. This is because extracting dyes from natural resources is a very sensitive process and needs specific conditions that may be hard to achieve (19). Another problem associated with natural dyes is that they are limited in both color range and quantities. One the other hand, synthetic dyes are prepared in laboratory. Their chemical structures could be adjusted to match the exact purpose of using them. Furthermore, they could be prepared on large scales for commercial use. Their main problem is that are not environmentally friendly to synthesize not to use (20, 21).

Due to the rapid increase of the production of synthetic dyes and their varieties, new classifications' techniques were needed. One suggested classification system categorizes dyes based on the functional groups that make up the chromophores within the dye. For example, Azo dyes which are the most common and important dyes have N═N functional, Nitro dyes have NO_2 functional…etc (15, 17). As mentioned earlier, dyes could be also classified cationic, anionic or nonionic based on the charge of the associate chromogen (22).

Due to the wide varieties of available dyes and their variant properties, specifically synthetic ones, dyes are involved in several fields. Besides being colorant and being an essential part of arts and painting, the most important field is the textile industry which is growing along with science of organic synthetic dyes (23). Dyes are used in the medical field as photosensitizers (24). They are also used as biological indicators for

cells (25). Furthermore, several dyes classes such as azo dyes that are part of the pharmaceutical industry and drugs synthesis (26). Further, they are used in the food industry to make food products more appealing (27), and they are used widely in the cosmetics industry (28). In analytical chemistry, dyes are used generally as colorimetric indicators (29, 30). They are used as pH indicators (29) and to detect metal ions as well (30).

1.2.1.1 *Xylenol Orange*

Xylenol orange, XO, is a synthetic organic acidic dye with a molecular formula of $C_{31}H_{32}N_2O_{13}S$. As reported by Nakayama et al., Xylenol Orange could be synthesized with high purity for commercial uses from cresol red (31) which is triarylmethane dye (32), iminodiacetic acid, anhydrous, and sodium acetate under acidic conditions (31). Xylenol Orange changes color upon changing the concentration, it is red in the concentrated solutions, and orange in the low concentrated solutions. Table 1.1 summarizes Xylenol Orange chemical and physical properties.

Table 1.1

Chemical and physical properties of Xylenol Orange sodium salt(33)

Feature	Xylenol Orange Sodium Salt
Chemical structure	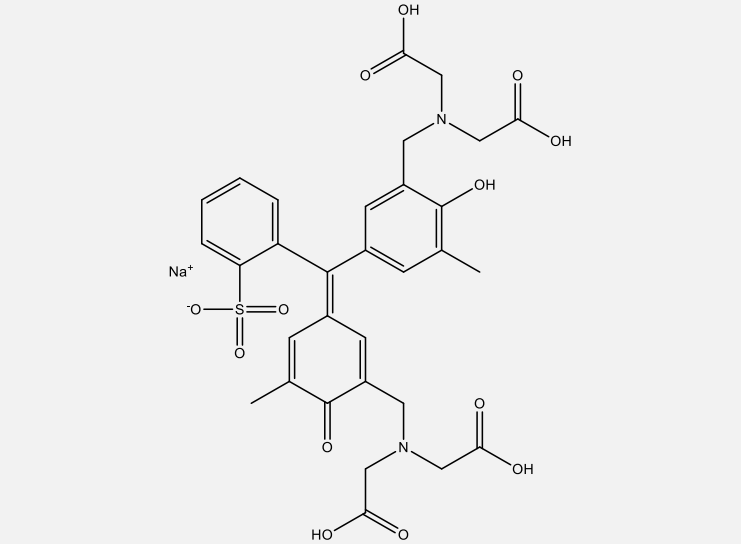
IUPAC name	sodium;2-[(E)-[3-[[bis(carboxymethyl)amino]methyl]-4-hydroxy-5-methylphenyl]-[3-[[bis(carboxymethyl)amino]methyl]-5-methyl-4-oxocyclohexa-2,5-dien-1-ylidene]methyl]benzenesulfonate
Molecular Weight	694.6 g/mol
Molecular Formula	$C_{31}H_{31}N_2NaO_{13}S$
Color	Yellow in pH<7 , purple pH>8
Solubility	Water soluble
CAS	63721-83-5

Besides being used in textile and printing industries as most of the dyes do (34), Xylenol Orange is widely used as a colorimetric indicator in metal titrations, displaying a yellow color in acidic medium and a purple color in basic medium (30). It could be used in both detecting and quantifying metal ions. This detection happens due to the ability of Xylenol Orange to form metal complexes, which changes the color of the pure Xylenol Orange (35). Hence the spectrum of the solution is also changing. In its UV-Vis spectrum, pure Xylenol Orange has two main peaks, at 433 nm and 573 nm (36). The absorption maximum is at 433 nm in the acidic mediums indicating its yellow color, and at 573 nm in the basic mediums indicates its purple color. In 2014, Belleza and Villaraza have proved the colorimetric abilities of Xylenol Orange in to detecting ion metals as Zn^{+2} at very low concentration levels below 1µM. This is a result of the complexation tendency of xylenol Orange with metal ions (30).

Xylenol orange is used in medicine as a fluorescent marker to detect the growth of bones and hard tissues (37), to determine the concentration of some drugs and remove the oxidized parts as in the case of indomethacin hydrazide(38). Also, research done by Smith et al. have showed the possibility of synthesizing Fricke gel of Xylenol Orange that could be used safely in modifying radiation dosimeters(39). Furthermore, Xylenol Orange could be used in purifying water from metals by forming easily separatable metal complexes (39). One of the most important feature of Xylenol Orange was stated by Li and Lin, that due to its organic structure along with its high solubility in water, Xylenol Orange is often used as a reference method that could be utilized in further studies (40).

On the other hand, Xylenol orange could be considered a chemical hazard. Xylenol Orange dye has negative effects on various humans' organs (41). Ingestion and inhalation of Xylenol Orange has harmful effects. Skin and eyes' contamination cause irritation. Additionally, it affects the nervous system, kidneys, and causes some blood illnesses (34). Also, it has irritation effects on mucosal tissues and the upper respiratory tract (42). Furthermore, Xylenol orange is considered as a water waste, since it can react with heavy metals to form harmful complexes that affects both humans and aqua environment (43, 44). In addition, it can inhibit bacteria growth (45). As Fa and Miao have reported, purification of Xylenol Orange from water, specially by photodegradation, is a challenging process (41). In addition to the negative impacts of Xylenol Orange presence in water, the difficulty of removing the dye from water complicates resolving the issue.

1.3 Water Quality Indices

As previously mentioned, not all water contaminations could be detected directly from the color, smell, and taste of water. Hence, more advanced and accurate indications for water quality are needed. One example is the Water Quality Index(WQI) , which is a method used to classify the quality of drinking water and indicates if it is safe and suitable to consume (46, 47). The first WQI was established in 1960 (46). Nowadays, there are at least up to 35 models of water quality indices which differ in the number of parameters included depending on the geographical region of interest. After collecting the needed data related to a certain groundwater source, the index will use several formulas and integration that generate a specific numerical value which could be used in

determining the quality of water. The index is designed to help indicate the level of contamination with water, and how it is affecting the quality of water (46, 47). For instance, a calculated numerical value of 100 in “the Weighted Arithmetic Water Quality Index Method” indicates that it is not safe to drink this water, while the best water quality is indicated by a value of zero (47).

Water Quality indices’ parameters generally study the chemical, physical, and biological properties of water. The most important parameter is Total Dissolved Solids (TDS) since it works as an indication for other parameters, without the need of including them in the calculation. Usually, pH measurement and Electric Conductivity are considered in almost all models (48). Some parameters as dissolved oxygen (DO), biological oxygen demand (BOD), and free CO_2 are very important parameters to evaluate the water quality for aqua life. Additional studied parameters could be total hardness, alkalinity, presence of metals such as iron, calcium, magnesium and arsenic. Furthermore, both presence and concentration of halogens such as chloride and fluoride are recorded (48, 49).

Meanwhile, there are several limitations and challenges associated with water quality indices. One problem is that the calculated value does not consider the uncertainties. There are several factors that may lead to errors while considering the index calculations. Also, the different models are not universal and choosing the right model might be confusing (49). Meanwhile, some parameters are given more importance than others while calculating the index value. Hence, some results could be misleading due to the fact that some contaminations could have minimal effect on the calculated value even at high concentrations. Furthermore, the interaction among different parameters and the influence of one parameter on other parameters is not taken into account. Hence, modifications are needed to make universal and more accurate (50).

1.4 Zero Discharge Policy

The industrial development is associated with a rapid increase of water consumption since the industrial sector is one of the major water consumers. Hence, it is essential to investigate industrial techniques that reduce both water consumption and waste generation. Zero discharge policy aims to limit the waste generated and discharged, which will reduce pollution expansion. This approach was investigated in the 1990s

directing to limit the huge amount of chemicals generated then discharged to seas water by the oil and gas industry. This would be achieved though restructuring the drilling and cleaning operations in approaches that use less chemical, replace harmful chemicals with less polluting reagents, and enhances recycling policies (51). The coal industry is as important as the oil and gas industry nowadays. It also consumes large water quantities. The latter results in high mining costs for companies, along with excess waste generation that increases water pollution levels. As Zhang et al. have illustrated, mining water could be treated to lower the pollution factors in wastewater, which will result in reusable water that could be used in further mining cycles. This approach is considered as both environmentally friendly and cost effective. Suggested treatments are considering prefiltration techniques via a membrane, hardness removal by using chemical agents to precipitate ions species such as calcium, and turbidity removal through mechanical filtration to discard solids (52). The use of water will be like a loop, same portion of water is used several. As a result, the consumption of fresh water is minimized (53).

1.5 Wastewater Purification Techniques

As discussed earlier, water pollution is a serious crisis that needs to be solved. Due to the variety of pollutants' both chemical and physical structures, many techniques have been developed aiming to improve the water quality. These techniques could be biological, physical or chemical treatment techniques (54).

Physical techniques, often referred to as primary treatment (55), tend to purify water from the different contaminations without affecting or changing the properties of the pollutants (56). They aim to minimize the biochemical oxygen demand present in water samples. No chemical reagents are needed to apply this sort of treatment. Physical techniques only aim to separate the pollutants from water without any modification on their structures. Usually, physical treatments are applied prior to biological and chemical techniques. It is preferred to start with pre-physical treatments such as screening, sedimentation, and skimming. Such steps aim to purify contaminations with large particle sizes. After that, more advanced techniques are used like membrane filtration, thermal treatment, and physical adsorption. Such techniques are efficient in separating the small contaminations in the nano scale (56). Even though such techniques as physical adsorption are very effective, they are also very selective in a negative way;

that each technique is limited to certain pollutants and could not be applied on variant pollutants. In addition, it is hard to separate the absorbent and the pollutant after the treatment, so the adsorbent will be considered as an additional waste. Meanwhile, in the case of membrane filtration, even the process is not selective, but a sludge could be formed which will reduce the efficiency of the membrane filter, hence the membrane should be replaced with a new one (57). Usually, more than one technique are combined together to obtain reliable results. Hence, treated water will be subjected to a series of coagulation-flocculation-sedimentation-filtration processes (58). It should be noticed that the effluent obtained from the primary treatment will be subjected for further secondary treatments , since such treatment are insufficient in removing all organic components (55).

Secondary treatments usually consists of biological treatments that aims to reduce the organic pollutants along with the levels of BOD associated with their presence in water (59). Biological techniques are considered to be low-cost techniques which are environmentally friendly. These techniques help in purifying water from pharmaceutical and metal wastes (55, 60, 61). There are several biological water treatments techniques including biodegradation (56). Moving bed bioreactors are an advanced biological method that uses biofilms to degrade the organic pollutants (59, 62). These bioreactors provide a high surface area for purification which increases efficiency. They are also considered as an economical technique since no backwashing is needed. Also, biofilms could be used several times with affecting the efficiency. In addition, they could be used on large scales and applied in the industrial field and in sewage treatments (62). Other biological treatments are purification with microorganisms, biofilters, and denitrification. Also, there are many bio adsorbents so the contaminations are being adsorbed on the walls of the cells (60). Moreover, bacteria and fungi can work as reducing agents which reduce metal ions to nanoparticles (63). Some limitations of the latter are that they work with only certain types of metals and only work in the nano scale (63).

Chemical techniques commonly require additional chemicals to be added to the treatment medium. Hence, the purifying chemicals and pollutants have a direct interaction via a chemical reaction, and the structure of the pollutant will change (56, 64). There are several chemical techniques as ion exchange, chlorination,

electrochemical treatment, UV radiation, ozonation, precipitation, and oxidation. Oxidation is the most common and used technique (56).

1.5.1 Advanced Oxidation Process

Oxidation treatments have been given an interest as being an advanced treatment method that is effective in breaking the toxic organic pollutants in water. Glaze et al. have investigated that oxidation depends mainly on generating hydroxyl radicals $HO^{\bullet}$ at certain levels of concentrations while being treated at normal conditions of temperature and pressure. In addition, it was noticed that the various sorts of light radiation such as UV and sunlight have positive effects in improving the oxidation efficiency (65).

Meanwhile, advanced oxidation process (AOP) involve the addition of strong radical oxidants as $OH^{\bullet}$, $SO_4^{\bullet -}$ to speed up the removal of organic pollutants (66). AOP methods involve electrochemical oxidation, photocatalysis, peroxonation, photo-Fenton, and ozonation. In general, chemical treatments are more advanced and more efficient in purifying water than biological and physical techniques (56, 64, 65). Fenton treatments use H_2O_2, coupled with iron catalyst in acidic mediums reaching a pH below 3. The reagent will start a sort of degradation for the organic pollutants. Moreover, this type of treatment is very efficient in purifying water from dyes on industrial levels. Peroxonation is also an efficient oxidation method that requires coupling H_2O_2 with O_3. As a result, O_3 activity will be enhanced leading for better removal of the micropollutants (65). Meanwhile, combining ozonation and UV radiation will result in active hydroxyl radicals that may work as an oxidation system (58). On the other hand, most of these treatments are expensive, since they are both reagents and energy consuming. Furthermore, as investigated by Dr. Badran et al. that toxic side products may be formed during the treatments , hence, advanced oxidation process are not favored and insufficient (67).

1.6 Photodegradation

Commonly known as light induced degradation, is a chemical process where colorants' molecules absorb photons lightened by different sources such as LED, sunlight, and UV irradiation (68). Since sunlight is renewable, free of charge, and environmentally friendly, it is favored over other light sources.(69); Due to the effect of photons emitted by light, molecules start degrading into new smaller molecules, these new molecules

will have different chemical and physical properties (70). Since no chemical reagents are needed here, the effectiveness of photodegradation depends mainly on the wavelength and intensity of the used light source, presence of oxygen, and exposure time to radiation(68). In general, the temperature of the medium will have no or minimal effect on the degradation process, since the thermal energy is not comparable with the one generated by photons (71). Unfortunately , it has a negative impact in art fields since it makes paintings faint(68). Meanwhile, adding photocatalysts may help increasing the efficiency of the degradation (68). This process works perfectly as wastewater treatment for dyes and other organic pollutants. On the other hand, some organic molecules as azo dyes may generate more toxic compounds upon degradation (72).

1.6.1 Photocatalysis

It is one of the most well-known AOP techniques (66). This approach refers to a modified version of photodegradation process where a photocatalyst is needed beside the light source to enhance the production of reactive oxygen species. Hence, organic pollutants degrade into smaller new compounds with greater efficiency. Photocatalysis begins with the interaction between the catalyst and the organic waste where the photocatalyst adsorbs the pollutant on its surface area. The efficiency of photocatalysis depends on both the light source and the photocatalyst. Both the intensity and wavelength of the light source influence the degradation efficiency. Regarding the photocatalyst, the nature of the catalyst mainly its surface area and its band gap are important. Meanwhile, the energy of the light source should be larger than the band gap of the used photocatalyst in order to activate it (69). Since it is preferable to use sunlight in photodegradation, photocatalysts with small band gaps are superior. As a result, photocatalysts containing semi-conductors within their structures, such as ZnO, CuO, Fe, Ag_2O are preferable because they are considered as solar active material with small band gaps (69, 72). A recent study for Tome at al. has reported that porphyrin groups which containing metal ions, such as Zn, Cu, and Ag, within their structures have the ability to photodegrade various organic pollutants under sunlight radiation while reaching a photodegradation rate of 100% (69).

As shown in Fig 1 in the appendix, photocatalysis starts when the photocatalyst absorbs the radiation from the light source. If the energy of the light source is greater than the

energy of band gap of the catalyst, the electrons in the valence band of the photocatalyst will be excited and move from the valence band up to the conduction band (73). For each electron moving to the conduction band, a positive hole will be generated in the valence band. Then, the positive holes and the negative electrons will move to the surface of the photocatalyst and work as active sites. Hence, two reduction reactions on the photocatalyst's surface will proceed forming two radicals, superoxide radical ($O_2^{\bullet}$) and hydroxyl radical ($HO^{\bullet}$) which work as active species to start the degradation of the dye (73).

Photocatalysis is very sensitive for several parameters. These parameters include both the wavelength and intensity of the light source (74), pH of the medium (75), the presence of oxidizing agents such as H_2O_2 (76), the amount of photocatalyst used (77), the initial concentration of the pollutants (77), and the nature of the photocatalyst (78).

Photocatalysis process is inversely proportional to the wavelength of the light source (74). Decreasing the wavelength of the light source increases the energy, which will result in photons with higher energy which will release more electrons. Hence the formation of hydroxyl radicals will increase, so the photodegradation rate will increase. Furthermore, increasing the intensity of the light source will increase the photocatalysis efficiency (79).

This is illustrated more in the following equations (73):

$$\text{photocatalyst} + \text{light}\left(E_{light} > E_{bandgap}\right) \rightarrow \text{hole}^{+} + e^{-} \qquad \text{Eq. 1}$$

$$\text{hole}^{+} + HO^{-} \rightarrow HO^{\bullet} \qquad \text{Eq. 2}$$

$$e^{-} + O_2 \rightarrow O_2^{\bullet} \qquad Eq. 3$$

$$hole^{+} + e^{-} + O_2^{\bullet} + \quad HO^{\bullet} + dye \rightarrow degradation\ products \qquad Eq. 4$$

Photocatalysis sequence reactions are very sensitive to the pH of the medium. The pH of the medium plays a dominant role in the electrical charge distribution of the photocatalyst's surface area, where reduction reactions happen (75). Hence, it is affecting the first step of photocatalysis, which is adsorption of the dye. Indeed, there is no preferred pH value that works the best for all photocatalysis. The optimal pH depends on both the nature of the dye and the photocatalyst (80). On the other hand,

there is a contradiction happening, that the oxidation of the positive holes that reacts to form the hydroxyl radicals tends to be formed more in the acidic mediums, while the hydroxyl radicals themselves prefers being formed in the basic mediums (81). Usually, the optimal pH depends on the point of zero charge of the photocatalyst. PZC is a property of solid catalyst that indicates the pH at which the surface of the catalyst would be neutral with no charge. Hence, mediums with pH exactly to the PZC of the photocatalyst are not preferred, since the interaction would be at its minimum, and no effective adsorption is observed. Meanwhile, at pH lower than PZC, absorption of H^+ is preferred and the surface of the catalyst would be positively charged, hence adsorption of anions is preferred. While at pH higher than PZC, the surface of the photocatalyst would be negatively charged, accordingly adsorption of the cations is preferred (80). In general, there is no specific rule for choosing the optimal pH , since it depends on the nature of combination of both the photocatalyst and the dye (81), it is a sort of trial and error that should be investigated from systematic analysis.

Adding oxidizing agents such as hydrogen peroxide (H_2O_2) and sodium hypochlorite (NaClO) enhances the efficiency of the photocatalysis degradation (76). Photodecomposition of oxidants as H_2O_2 will generate a reactive hydroxyl radical as the following equations show (81):

$$light + H_2O_2 \rightarrow 2HO^{\bullet} \qquad Eq.5$$

$$e^- + H_2O_2 \rightarrow HO^{\bullet} + HO^- \qquad Eq.6$$

Following, the hydroxyl radicals will attack the aromatic rings of dyes and oxides their functional groups, which improves the efficiency of degradation (76). Contrary, using excess hydrogen peroxide will decrease the efficiency of photocatalysis rather than enhancing it. This was a result of a study held by Feng and others, their photo-Fenton study in dye removal under UV radiation showed an increase in efficiency while adding H_2O_2. Contrary, a decline in the removal efficiency was noticed while exceeding an H_2O_2 concentration beyond 500 mg/L (79). This may be a result of consuming the hydroxyl radical by peroxide, as shown in the following equations (81) :

$$HO^{\bullet} + H_2O_2 \rightarrow HO_2^{\bullet} + H_2O \qquad Eq.7$$

$$HO_2^{\bullet} + \ HO^{\bullet} \rightarrow \ O_2 \ + H_2O \qquad Eq.8$$

Additionally, the used amount of photocatalyst affects photocatalysis efficiency (77). Increasing the used amount of catalyst in certain conditions of photodegradation treatment will speed up the process, since it increases the number of active sites of the catalyst. Hence, adsorption will be faster, and the number of hydroxyl radicals forming will increase, and the dye will degrade faster. On contrary, Increasing the amount of photocatalyst beyond a certain level will decrease the efficiency of degradation. This happened because the medium will be over saturated, hence the photons will not reach the active sites efficiently (77, 79).

The photodegradation rate also depends on the initial concentration of the dye. A study conducted by Chakrabarti and Dutta has confirmed that increasing the concentration of the dye has a negative influence on the efficiency of photodegradation, since the solution will be more crowded. The latter will prevent light photons from reaching the active sites on the surface of the catalyst within the solution. Hence, the rate of photocatalysis will be decreasing (82).

Moreover, there are several semiconducting nanoparticles that could be used as photocatalysts. Usually, metal oxides such as ZrO_2, V_2O_5, CeO_2, Fe_2O_3, WO_3, and TiO_2 are used as photocatalyst. Also, sulfides such as CdS, PbS, and ZnS are commonly used in photocatalysis of organic pollutants (78).

1.6.1.1 Titanium Oxide

Titanium oxide TiO_2 is an n-type semiconductor which is involved in many technological and environmental applications. It occurs in nature in three different phases: rutile, anatase, and brookite (42, 83). The rutile phase is the most stable and common phase. Hence, most studies consider the rutile phase. Rutile TiO_2 has a large band gap equal to 3.02 eV, corresponding to a wavelength of 410 nm in the visible region. On the other hand, anatase is more active and works better in the oxidation - reduction reactions, but it has one limitation that it absorbs in the UV region (83). Meanwhile, brookite is usually not considered, since it is no common to find it in its pure form; it convert to the rutile form with heat (84). TiO_2 is used widely in water purification treatments as both adsorbent (42) and as a photocatalyst (83). Its photocatalytic efficiency was proven for the first time in 1932, since then, it has been

considered as the golden photocatalyst. This is because of its wide availability, economical, environmentally friendly, and its chemical stability (83).

One main drawback of TiO_2 as a photocatalyst is the possibility of recombination among the positive holes and the negative electrons on its surface. As a result, they will not be involved in the reductions reactions, which will lower the photocatalytic efficiency (85). This recombination happens fast that only 10% of the generated holes and electrons will stay separated. The main reason for hole-electron recombination is the defect sites of surfaces happening due to oxygen vacancies. The latter will make the surface of the catalyst electron rich. Accordingly, the distribution of the charge will change, and the interaction with the dye will decrease(83). Another problem associated with titanium oxide is the hard purification techniques. Even though it purifies water from dyes, removing TiO_2 from water after the photodegradation treatment is complicated because TiO_2 sours the solution. Therefore, modifications that improve its morphologies are needed (86).

Using TiO_2 in the forms of nanotubes, nanosphere, nanofibers are preferred over pure TiO_2 (86). It was found that using TiO_2 in the nano scales increases its removal efficiency for dyes and other pharmaceutical pollutants. The charge of the nano particles will behave according to the law of quantum chemistry. This will result in a large band gap, and formation of the positive holes and the negative electrons will increase. Thus, the rate of reduction reactions will be faster. Meanwhile, the TiO_2 nanoparticles have a porous surface which enhances the active surface area. Also, its surface will be capturing more HO groups, so it enhances the formation of $HO^{\bullet}$, hence the degradation efficiency increases (87).

The most common modification of TiO_2 is doping TiO_2 with other metal oxides such as ZnO, CuO, and Fe_3O_4. Metal oxides have low band gap, so they can absorb light in the visible region. Due to the paramagnetic feature of some metals as iron, the recovery of the photocatalyst after treatment will be easier, since a strong magnate could be used to remove the catalyst from the solution (86). On the other hand, such compounds are unstable when exposed to radiation. Doping TiO_2 with metal oxides will lower the band gap of TiO_2 and increases the stability of the metal oxides (88). For example, a recent study done by Khan and others has showed that the band gap of TiO_2 was dropped from 3.22 eV to 2.84 eV by doping TiO_2 with Cr nanoparticles, while increasing the

photocatalytic properties of titanium oxide (89). Also, doping increases the efficiency of TiO_2 by decreasing the tendency of recombination between electrons and holes that occurs in the case of pure TiO_2. Research by Sherly et al. has investigated that doping with metals such as Ag will reduce the recombination rates among the negative electrons and positive holes. This is a result of the potential energy barrier that is called Schottky barrier; this occurs due to the interaction between species that differs in their band gaps as Ag metal and TiO_2 particles (86). Even though doping increases the stability of metal oxides, they will not be stable in the long term (88). Meanwhile, other modifications such as surface deposition may result in more stable compounds (88).

1.7 Fe_3O_4 Nanoparticles

Iron oxide nanoparticles, specifically Fe_3O_4(magnetite), are well-known for their exceptional magnetic properties, electronic conductivity, and biocompatibility. Fe_3O_4 has a cubic inverse spinel crystal structure containing iron in two oxidation states, Fe^{2+} and Fe^{3+} (90). Meanwhile, synthesis methods of Fe_3O_4 influence its morphology, crystallinity, and surface properties, which in turn affect its paramagnetic characteristics (90, 91). For example, thermal decomposition and solvothermal produce spherical superparamagnetic nanoparticles. Meanwhile, thermal decomposition of iron (III) oleate with sodium oleate surfactant yields superparamagnetic cubic Fe_3O_4 (90). Other synthesis techniques include Co-precipitation method, hydrothermal method, Polyol method, and electrochemical deposition method (91). Each synthesis method affects the properties of Fe_3O_4 nanoparticles, making them suitable for various applications in separation technology, catalysis, medical science, and environmental fields. However, a drawback of Fe_3O_4 nanoparticles is their high chemical reactivity, which can lead to surface oxidation. Therefore, stabilizing the surface is crucial to preserving their paramagnetic properties (91).

1.8 Aims of the study

The aim of the study is to prepare magnetic nano particles that can work as photocatalysts. The nano particles are prepared from doping TiO_2 with the paramagnetic nano particles of Fe_3O_4, under basic conditions. The new synthesized catalyst will be used for water treatment of Xylenol Orange dye under visible radiation conditions. This is the first study aiming to synthesize 10%TiO_2/Fe_3O_4 and use it as a photocatalyst for Xylenol Orange under LED radiation. The doping technique aims to decrease the band

gap of TiO_2; accordingly, it will be active under visible radiation. Furthermore, the magnetic features of Fe_3O_4 will allow a simple post treatment purification with a strong magnate.

The PZC of the synthesized photocatalyst from doping TiO_2 with Fe_3O_4 will be studied. Also, the photocatalysis effect of the newly prepared catalyst will be compared to the ones from both Fe_3O_4 and pure TiO_2 in the rutile form. Different parameters affecting the photocatalysis in presence of 10%TiO_2/Fe_3O_4 will be studied including the effect of LED radiation, exposure time, pH of the medium, amount of the photocatalyst, concentration of the dye, presence of H_2O_2, optimal conditions, and photocatalyst recovery and reuse. In addition, the rate order of photocatalysis reaction will be studied through kinetics. Furthermore, the photodegradation mechanism will be studied by using density functional theory (DFT).

Chapter Two
Experimental

In this chapter, the methodology of the study will be discussed in detail. The first part will discuss the preparation of the photocatalyst of 10%TiO_2/Fe_3O_4. The second part will discuss the photocatalysis reaction and the different parameters affecting the degradation will be studied. The detailed experimental work, chemical reagents, equipment, and data collection process will be discussed while highlighting the importance of each step.

All of the experimental work was done at the chemistry laboratories of An-Najah National University. All pH measurements were done at room temperature using JENWAY 3510 pH meter. All used solids were weighted using MRC analytical balance ASB-310-C2-V2. Atomic force microscope (AFM) images were done using a CoreAFM produced by Nanosurf, Switzerland. The tapping mode was used with a force constant of 5 N/m and a resonance frequency of 150 kHz (92). Then, AFM images were generated and Gwyddion software. All UV-Vis spectra were recorded in the range of (350-700) nm in triplicates by a SHIMADZU UV-1800 spectrophotometer, then averaged using Excel program. UV-Vis and pH results mentioned in this work were also obtained at An-Najah laboratories. Meanwhile, GC-MS analysis was done using (GCMS, QP5000, Shimadzu) equipped with AOC-20i autosampler with a general purpose 5% polar column (Alltech Heliflex® AT™-5ms, 30 meter).

The catalyst was prepared using Iron (II) ammonium sulphate ($Fe(NH_4)_2(SO_4)_2.6H_2O$) that was purchased from CARLO ERBA reagents company, Italy, Ammonium Iron (III) sulfate dodecahydrate ($NH_4Fe(SO_4)_2\cdot12H_2O$) obtained from Riedel-de Haen company that based in Germany, Titanium(III) chloride ($TiCl_3$) 12% solution was purchased from Sigma-Aldrich that based in USA, 25% Ammonia solution (NH_4OH) from Loba Chemie based in India, and 99% ethanol (C_2H_6O) was purchased from Sun Pharm drug store which is based in The West Bank. Also, the universal drying oven LOD-O6OE from LabTech was used to dry synthesized catalyst. Sodium nitrate ($NaNO_3$) and sodium hydroxide solution (NaOH) were purchased as solids from Frutarom company based in Haifa, and 70% nitric acid (HNO_3) was obtained from SDFCL - SD Fine Chemicals that based in India were used in determining the PZC of the catalyst, and by

using Lab Tech® shaker (DaihanLabtech). Titanium oxide (TiO_2) in the rutile form was purchased from Aldrich company. Titanium oxide was extracted from the aqueous solutions by using Low speed centrifuge LLS-A12 from labtorn.

Xylenol Orange was used in the form of Xylenol Orange Sodium Salt as a pollutant in this study. The dye was purchased in the form of a solid powder from Alpha Aesar, based in the United States, with CAS of 63721-83-5. Multiple fresh stock solutions of Xylenol Orange with different concentrations were prepared for each experiment separately. The initial pH of the dye in distilled water was found to be ~5.5. Only when needed, the pH of the solution was adjusted by using Acetic acid, NaOH solution, ammonia solution, or ammonia buffer with pH equal to 10. Pure Acetic acid was purchased from Sun Pharm drug store baes in The West Bank, and ammonia buffer was prepared from ammonia solution and ammonium chloride which were purchased from Loba Chemie, which is based in India. In addition, Hydrogen peroxide (H_2O_2) solution was used as an oxidizing agent and purchased from Sun Pharm drug store based in The West Bank.

All photocatalysis experiments were held under 100W LED in closed transparent plastic cups while stirring as shown in Fig 2 in the appendix. Also, all experiments were done at room temperature while stirring.

2.1 Catalyst Analysis

2.1.1 Catalyst Preparation

Preparation aims to dope TiO_2 with the magnetic Fe_3O_4. The percentage by mass of TiO_2 to Fe_3O_4 in the prepared catalyst will be equal to 10%. As mentioned earlier in section 1.6.1.1, doping TiO_2 with paramagnetic metals reduces the band gap of titanium oxide and makes the recovery of the catalyst easier upon treatment.

To prepare 0.3 mol of Fe_3O_4 doped with 10% by mass TiO_2, a 1000 ml beaker that was placed on a hotplate stirrer under the hood. 200 ml of distilled water was heated up to at 60◦ C. Then exactly 11.76g of Fe $(NH_4)_2$ $(SO_4)_2.6H_2O$, 28.93g Fe (NH_4) $(SO_4)_2.12H_2O$, and 9.31 ml of $TiCl_3$, were added to the preheated water. Ammonium hydroxide solution was added gradually while stirring to ensure having a basic medium with pH >10. The reaction was held for 90 minutes while stirring at 60-50◦C and a pH < 10.

The black magnetic nano particles will have the molecular formula of 10%TiO_2/Fe_3O_4. After the reaction was done, the formed product was put aside to settle above a strong magnate. Once the nano particles settled, decantation was performed to remove the immiscible liquid. To ensure removing all the impurities were in the immiscible liquid, the obtained product was subject to several washing cycles. The nano particles were washed first with distilled water then with pure ethanol. The washing solutions were also decanted, then the nano particles were collected and put in the drying oven at 75º C. Once they are dry, the nano particles are grinded by ceramic mortar and pestle. The nano particles weighing 9.56g were collected in a plastic reactor and kept in the dark for further use.

2.1.2 Catalyst Characterization

2.2.2.1 AFM Analysis

The aim of our study is to synthesize nanoscale particles to enhance the surface area and photocatalytic properties. To confirm the nano scale features of our catalyst, atomic force microscopy (AFM) will be used to study the surface area of the catalyst. AFM analysis is very essential and rapid method for studying both the topography of materials surfaces along with their sizes. The detailed images provided by AFM helps observing the distribution of the particles, their morphology, and indicates any possible aggregation (93).

2.2.2.2 Point of Zero Charge

As mentioned earlier in section 1.6.1, PZC affects the nature of the photocatalyst, hence influences the photocatalysis process. As a result, studying PZC of the synthesized catalyst is very important. The procedure of Bakatula et al. was followed (94). 0.1 M $NaNO_3$ solution was prepared by dissolving 8.5g of $NaNO_3$ in a 1.0 L volumetric flask. Eleven 50 ml centrifuge tubes were prepared by transferring 40 ml of the later solution in each tube. Then, the pH was adjusted by using 0.1M HNO_3 and 0.1M NaOH solutions to obtain a pH range from 2 up to 11. The initial pH for each tube was recorded precisely, then 0.1g of the previously prepared catalyst of 10%TiO_2/Fe_3O_4 were added to each tube. All tubes were left in the shaker for 23 hours at room temperature and 250 RPM. The final pH of each tube was recorded.

2.2 Photodegradation Process

2.2.1 Effect of Time

The aim of the study is the determination of the photocatalytic degradation of Xylenol Orange dye. Also, to study the kinetic of the reaction and investigate the rate order of the photocatalysis process. Hence, a 50 ppm Xylenol Orange solution with an initial pH of 5.09 was freshly prepared. 25 mg of Xylenol Orange dye were accurately weighted and transferred into a 500 ml volumetric flask, then dissolved with distilled water. Each condition was performed in duplicates to ensure accuracy.

A total of 6 plastic reactors were prepared. 25 ml of the 50 ppm Xylenol Orange solution was transferred to all reactors. 2 reactors were left with no further adjustments. In the second set that consists of 4 reactors, 10 mg of photocatalyst of 10%TiO_2/Fe_3O_4 were added. All reactors were closed. Two reactors from each set were put under LED radiation while stirring. The remaining 2 reactors were put in the dark. The UV-Vis spectrum for all reactors were taken with time for 3 days in triplicates.

2.2.2 Effect of Doping on the Photocatalytic Properties of TiO_2

As mentioned earlier in section 1.7, the aim of this study is to synthesize a new photocatalyst that is active under LED and easy to purify after the treatment. This should be achieved by doping. Hence, it is important to compare the effect of the magnetic photocatalyst to the rutile TiO_2, to examine if both have the same impact and mechanism on photodegradation.

In this study, while all conditions are identical, different photocatalysts were used. Equal amounts of rutile TiO_2 and 10%TiO_2/Fe_3O_4 were added to two sets of plastic reactors, and changes in the spectrum were recorded with time. To ensure better accuracy, the study was performed in duplicates.

50 ppm of Xylenol Orange solution was prepared with pH equal 5.5. Two reactors were prepared by adding 25 ml of the Xylenol Orange solution to 10mg of TiO_2 and a stirrer bar. Another two reactors were prepared by adding 25 ml of Xylenol Orange and 10 mg of 10%TiO_2/Fe_3O_4 Catalyst. All samples were put under LED while stirring for 3.5 hours. A strong magnet was used to purify the solution from 10%TiO_2/Fe_3O_4.

Meanwhile, centrifuge for 4 minutes at 4000 RPM was used to separate TiO_2. Finally, UV-Vis spectrum was taken for all samples in triplicate.

Percent change in absorbance with time at Xylenol Orange's peak at 433 nm and the intermediate's peak at 578nm were plotted along with their errors.

2.2.3 Effect of Doping on the Photocatalytic Properties of Fe_3O_4

As mentioned in section 1.6.1.1, doping TiO_2 with metals will result in a decrease in the band gap of titanium oxide. Hence, it is important to study the enhancements that are added to the magnetic nanoparticles of Fe_3O_4 once doped with TiO_2. In this study, while all conditions are exactly the same, but the catalyst used, equivalent amounts of Fe_3O_4 and $10\%TiO_2/Fe_3O_4$ were added to two separated plastic reactors, and changes in the spectrum were recorded. To ensure better accuracy, the study was performed in duplicates.

50 ppm of Xylenol Orange solution with pH equal 5.5 was prepared. 25 ml of the later solution were added to two reactors containing 10mg of Fe_3O_4. Another two reactors were prepared by adding 25 ml of Xylenol Orange and 10 mg of $10\%TiO_2/Fe_3O_4$ Catalyst. All reactors were closed then put under LED while stirring for 3.5 hours. A strong magnet was used to purify both solutions. Then, UV-Vis spectrum was taken for all samples in triplicate. The average spectra with time for each set of samples were plotted.

2.2.4 Effect of Amount of the Catalyst

It is very important to determine the ideal amount of photocatalyst to be used in the degradation process. Since using excess catalyst will increase the cost of the procedure. Besides, large amounts of the catalyst may result in enhancement of an adsorption treatment instead of degradation. To enhance the reliability, the experiment was done in duplicates. Also, control samples were put in the dark to study the effect of LED separately.

In this experiment, 50 ppm of Xylenol Orange solution was freshly prepared. The pH of the medium was adjusted with 0.1 M NaOH to reach the neutral condition with pH=7.01. 25 ml of the previously prepared solution was transferred into 24 closed reactors, then grouped into sets of four. Different amounts of catalyst were added to

each set. The amounts were 0 mg, 10 mg, 20 mg, 30 mg, 40 mg, and 50 mg. Two of each set were put in the dark as control samples and the other two were put under LED while stirring. The UV-Vis spectra for all samples were recorded in triplicate after 1 hour.

2.2.5 Effect of Solution's pH

As mentioned earlier in section 1.6.1, it is hard to predict the optimal pH where the photocatalyst works the best. Meanwhile, choosing a pH that is not equal to the PZC is a must. Accordingly, the photodegradation was analyzed at five different pHs. This study was held in duplicated while applying identical experimental conditions but changing the pH.

1.0 L stock solution of 50 ppm Xylenol Orange was prepared with an initial pH of 5.55. Then, different solutions were prepared by adjusting the pH of the stock as shown in Table 2.1.

The effect of pH was studied at different conditions. The first condition is the presence of the catalyst. Hence, two reactors containing 20 mg of 10%TiO_2/Fe_3O_4 and 25 ml 50 ppm Xylenol Orange solution were closed and put under LED radiation while stirring for 1 hour. Another two reactors were prepared with the same conditions but were put in the dark. To study the effect of LED alone, two reactors containing only 25 ml of the Xylenol orange solution were put under LED, and another two reactors were put in the dark. After 1 hour, pH of all samples and UV-vis spectrum in triplicate were recorded for all reactors. The previous procedure was repeated 4 times while using different 50 ppm Xylenol Orange stock solutions with pHs of 3.3, 5.55 ,7.20 and 10.05 respectively.

Table 2.1

Data of pH adjustment of 50 ppm Xylenol orange

pH of the solution	Solution used for adjustment	pH after treatment	λ max
3.30	acetic acid	3.3	433 nm
5.55	-	5.53	433 nm
7.20	0.1 M ammonia solution	7.19	433 nm
9.10	0.1 ammonia solution	8.12	578 nm
10.05	Buffer 10 of ammonia and ammonium chloride (NH_4Cl)	8.83	578 nm

2.2.6 Effect of Initial Concentration of Xylenol Orange

As mentioned earlier in section 1.6.1, concentration of the dye affects the efficiency of photodegradation. Hence, it is important to study the range of concentrations at which photocatalysis will be efficient. Since too saturated solution works as blockage for photons of light, which will prevent them from reaching the surface of the photocatalyst, hence it will not be activated. As a result, photodegradation will be less efficient (82).

100 ppm Xylenol Orange stock solution was prepared. Different dilution factors of the stock were applied to prepare 5 different concentrations of Xylenol Orange solution. 10 ppm, 20 ppm, 30 ppm, 40 ppm, and 50 ppm solutions were prepared with dilution factors equal to 0.1, 0.2, 0.3, 0.4, and 0.5 respectively.

The next procedure below was repeated 5 times using the previously prepared Xylenol Orange solutions with concentrations ranging from 10 ppm to 50 ppm.

Three closed reactors containing 25 ml of Xylenol Orange solution were prepared. No further adjustments were needed on the first reactors. 10 mg of 10%TiO_2/Fe_3O_4 photocatalyst were added to the second and the third reactors. The first two reactors were put under LED while stirring. Meanwhile, the third reactor was put in darkness. The UV-Vis spectra for all samples were recorded before treatment in triplicates. Other spectra were also recorded after 4 hours of treatment in triplicates.

2.2.7 Effect of H_2O_2

As already stated in section 1.6.1, presence of oxidizing agents enhances the photodegradation process by generating more hydroxyl radicals. Accordingly, it is important to determine the optimal amount needed to be used from the oxidizing agent. Otherwise, excess presence of it will decrease the efficiency of photocatalysis for a higher cost.

In this study, hydrogen peroxide (H_2O_2) was chosen as an oxidizing agent. Four plastic reactors were prepared by adding 25 ml of 50 ppm of Xylenol Orange solution with initial pH =5.65. 10 mg of 10%TiO_2/Fe_3O_4 photocatalyst was added for each reactor. Then, 1 ml of 1% H_2O_2 was added to the first sample,1 ml of 2% H_2O_2 was added to the second, 1 ml of 3% H_2O_2 was added to the third, and the fourth was set as a control in absence of H_2O_2. UV-Vis spectrum was recorded for all samples with time for 3 hours in triplicates.

2.2.8 Optimal Conditions

An individual experiment was used to study the photocatalysis process at optimal conditions. As a result, one reactor containing 25 ml of 20 ppm Xylenol Orange solution was prepared. The pH was adjusted with acetic acid to reach a pH of 2.95. 1 ml of 3% H_2O_2 solution, and a 10 mg of 10%TiO_2/Fe_3O_4 catalyst. Were added to the latter solution The plastic reactor was closed and put under LED while stirring for 5 hours. The UV-Vis spectrum was recorded with time in triplicates.

2.3 Photocatalysis Mechanism

2.3.1 GC-MS Characterization

To ensure the formation of new degraded smaller compounds, GC-MS was performed for 20 ppm Xylenol Orange solution at its normal pH ~5.5. The analysis was performed on samples before and upon treatment with 10mg of Fe_3O_4.10% in presence of 1 ml of 3% H_2O_2. The same GC-MS experimental conditions used in Dr. Badran's et al. work were used in our study, but with different mobile phase (67). Helium was set to be the carrier gas. The mobile phase was chosen to consist of methanol; hence, the sample was diluted in methanol. Then, 2.0 microliters of the diluted solution were injected with a flow rate 1.5 mL per minute and a split ratio of 1 : 10. Meanwhile, the mass detector was connected to NIST mass spectral library 2014 to help identify the obtained peaks.

2.3.2 DFT Calculations

Density functional theory was used to confirm the photocatalytic mechanism. For the optimization the same functional of B3LYP used in the work of Dr. Badran et al. was used for this study (67). Meanwhile a more diffused basis set, ma-def2-SVP, was used. As proved by Si et al., the more diffused basis sets give more accurate enthalpy calculations for large molecules(95). Also, to be comparable with the environmental conditions of the photocatalysis process, CPCM solvation model with water was used in performing all calculations. Meanwhile, all the calculations were done using Orca 4.3 software.

2.4 Catalyst Recovery and Reuse

Photocatalysis is very important to enhance the quality of water. Meanwhile, it is important to obtain photocatalysts which are reusable; to decrease the cost and reagents used in the degradation process.

10%TiO_2/Fe_3O_4 catalyst was extracted from the various previously analyzed samples. The catalyst was collected by using a strong magnet. Then, three different solutions were used to wash the catalyst. The first amount of the recovered catalyst was washed with 2mM NaOH, the second with 2mM HNO_3, and the third with ethanol. The washing solutions were decanted. Then, the catalyst was set to dry in the drying oven at 75º C.

The previously washed and recovered catalysts were used in new photocatalysis cycles. The optimal conditions were performed. 20 ppm solution was used after adjusting the pH with acetic acid to reach a pH of ~3. Four reactors containing 25 ml of the later solution and 1ml of 3% H_2O_2 were prepared .10 mg of fresh 10%TiO_2/Fe_3O_4 were added to the first sample. 10 mg of the recovered catalyst with different washing solutions were added separately to the reaming three reactors. All samples were put under LED with stirring for 4 hours. The initial UV-Vis spectrum and the spectrum after 4 hours were recorded in triplets.

After the reuse cycle has finished, the catalyst washed with ethanol was extracted again. The catalyst was washed another time with ethanol and used in more photocatalysis cycles. Applying the same optimal conditions mentioned above, the catalyst was subjected to another two cycles of reuse.

Chapter Three

Results, Discussion and Conclusion

In this chapter, the synthesized photocatalyst of 10%TiO_2/Fe_3O_4 will be discussed in terms of its PZC. Also, different parameters affecting the photodegradation of Xylenol Orange with 10%TiO_2/Fe_3O_4 will be presented. The optimal conditions of this degradation along with the mechanism will be investigated. The effect of time, LED radiation, pH of the medium, concentration of Xylenol Orange, amount of catalyst, and presence of H_2O_2 will be discussed.

The mentioned results were obtained after following procedures mentioned earlier in chapter two and were collected as excel data sheets. Microsoft Excel was used to organize the collected data. Since all UV-Vis spectra were collected in triplicates and some parameters were studied as duplicates, the average absorbance was calculated along with the errors. Thus, all absorbance results mentioned in this chapter represent the averaged value. Also, Origin 2024 was used to plot and represent all spectra and graphs.

3.1 Catalyst Synthesis and Characterization

3.1.1 Catalyst Synthesis

10%TiO_2/Fe_3O_4 was successfully synthesized under basic conditions. The black magnetic crystals were formed, as shown in the following equations:

The first step is dissociation in water:

$$NH_4Fe(SO_4)_2 .12H_2O\ _{(s)} \xrightarrow{(H_2O)} NH^+_{4(aq)} + Fe^{3+}_{(aq)} + 2SO^{-2}_{4\ (aq)} + 12H_2O_{(l)} \quad \text{Eq.9}$$

$$Fe(NH_4)_2(SO_4)_2 .6H_2O\ _{(s)} \xrightarrow{(H_2O)} 2NH^+_{4(aq)} + Fe^{2+}_{(aq)} + 2SO^{-2}_{4\ (aq)} + 6H_2O_{(l)} \quad \text{Eq.10}$$

$$NH_{3(aq)} + H_2O_{(aq)} \rightarrow NH^+_{4(aq)} + HO^-_{(aq)} \quad \text{Eq.11}$$

Hence, the magnetic nanoparticles of Fe_3O_4 will be formed as indicated following:

$$2Fe^{3+}_{(aq)} + Fe^{2+}_{(aq)} + 4H_2O_{(aq)} \rightarrow Fe_3O_{4(s)} + 8H^{+}_{(aq)} \quad \text{Eq.12}$$

Also, $TiCl_3$ will be oxidized to form titanium oxide:

$$4H_2O_{(l)} + 2TiCl_{3(l)} \rightarrow 6HCl_{(l)} + H_{2(g)} + 2TiO_{2(s)} \quad \text{Eq.13}$$

The magnetic black nanoparticles were insoluble in water and ammonia mixture; thus, a strong magnet was used to collect them from the aqueous solution. Multiple washings with ethanol and water were performed, it was noticed that the nano particles did not dissolve in ethanol as well. The washing solutions were decantated. Then, the nano particles were dried in the oven and collected for further analysis. Hence, it was proven that the catalyst is not mixing nor dissolving with water but participate allowing easy purification techniques. In other words, the first goal of synthesizing the catalyst was achieved by getting a magnetic catalyst that is easy to purify post treatment. Meanwhile, the photocatalytic efficiency under visible light is going to be discussed next in detail in Section 3.2.

3.1.2 Catalyst Characterization

3.1.2.1 AFM Analysis

AFM was used in this study to study the surface morphology of the synthesized 10%TiO_2/Fe_3O_4 photocatalyst and to confirm its nanoscale features. As shown in Fig 3.1 (a), the high-resolution AFM image confirms the nanoscale features of our catalyst have a spherical shape with diameters between 30 and 40 nm. These nano particles are considered to be heterogeneous since they vary in both their size and height distribution over the surface. Meanwhile, AFM image shown in Fig 3.1 (b), shows a broader scale range up to 80 nm, which indicates nanoparticles aggregation. This implies that some nanoparticles cluster together due to the interaction between the particles upon synthesis, resulting in a heterogeneous nature of the catalyst. In summary, AFM images of the synthesized 10%TiO_2/Fe_3O_4 show nanoparticle aggregation while indicating a heterogenous nanoscale structure.

Figure 3.1

AFM images of 10%TiO_2/Fe_3O_4

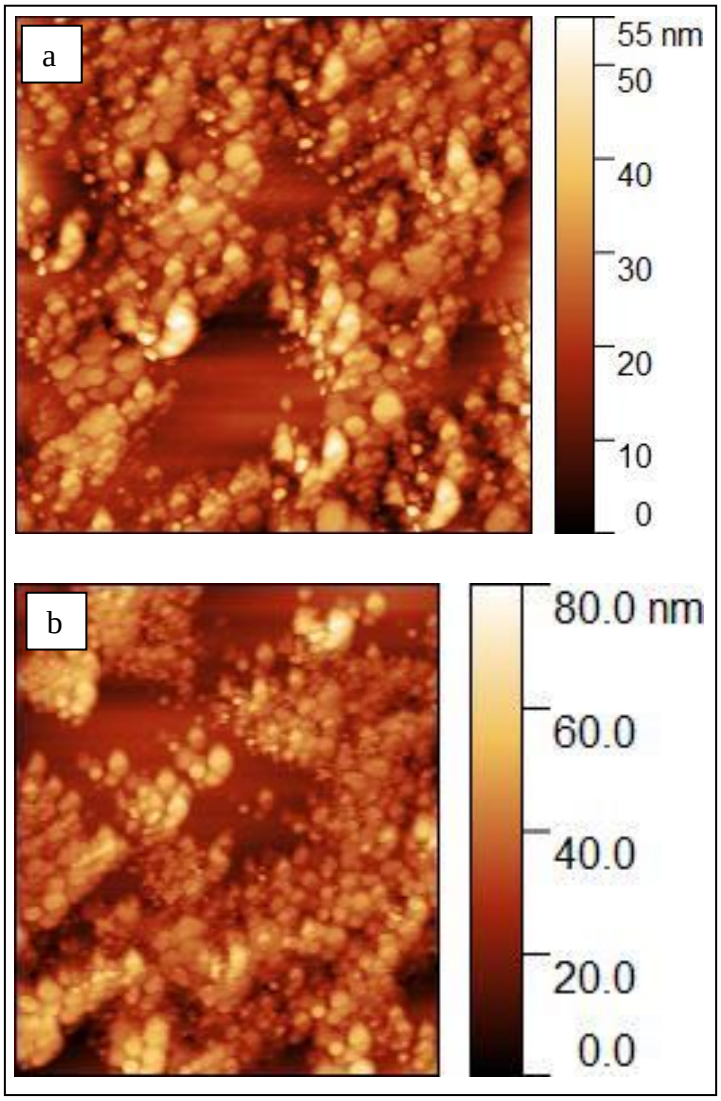

3.1.2.2 Point of Zero Charge

In this study, the pH of the ionic solution of $NaNO_3$ was adjusted with NaOH and HNO_3 solutions to obtain a pH range of (2-11). The final pH of the medium was recorded after 23 hours of adding 0.1 g of 10%TiO_2/Fe_3O_4. The change of the pH was calculated by applying the following equation,

$$\Delta pH = pH_f - \ pH_i \qquad Eq.14$$

In general, the synthesized catalyst had an acidic influence in most of pH ranges. A minimal increase in pH for tubes with initial pH < 5 was noticed. For samples with an initial pH > 5, a pH decrease was noticed. The change in pH versus the initial pH was plotted using origin, as shown in Fig 3.2. A horizontal line at y=0 was outlined. It was

noticed that the horizontal line intersects the previously plotted graph at 4.69 which indicates its PZC. In their recent study, Al-Salihi and others have found that the catalyst of m-TiO_2/Fe_3O_4 had a PZC value equal to 4.5 (96). Hence, the obtained PZC value in our study for 10%TiO_2/Fe_3O_4 catalyst is considered to be valid.

Figure 3.2

PZC plot of 10%TiO_2/Fe_3O_4

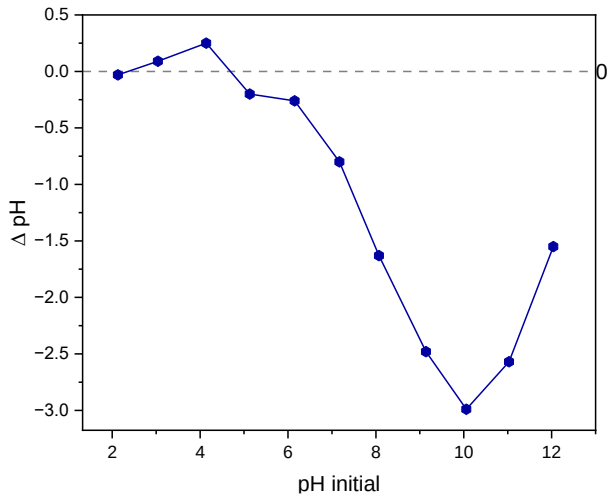

The PZC represents the pH value where the surface of the catalyst has no net charge; hence the surface is neutral. This is due to the equilibrium between the ions of H^+ and HO^- that are adsorbed on the surface. As a result, no interaction with the medium will happen. (97). Hence, photodegradation will not be efficient in mediums with pH that is equal to the PZC due to the low interaction levels. When going below the PZC, the surface of the catalyst will positively charge, which will increase interactions with the anions. On the other hand, a negatively charged will result when the pH of the medium is above the PZC(97) .

Due to the absence of adsorption of the charged anions and cations at a pH exactly equal to the PZC, the photocatalysis medium should have a pH significantly different from 4.69 to ensure the necessary electrostatic interactions for initiating the degradation. Meanwhile, the exact optimal pH needs more investigation to be identified. Hence, it will be discussed in the next section.

3.2 Photocatalysis

3.2.1 Effect of Contant Time

The effect of time was studied applying 3 different conditions. The first condition is in presence of LED as a visible light, in order to study the photodegradation possibility in absence of the catalyst. The second condition was applied to study the photocatalysis process in the presence of the previously prepared catalyst under the radiation of visible light. The last condition was applied to study the changes occurring by the catalyst in absence of any sort of traditions.

For the first condition studying the photodegradation process under visible radiation, 25 ml of 50 ppm solution were put in a closed plastic reactor under LED and the UV-Vis spectrum was recorded with time. This represents a photodegradation process where photons of light may have the ability to break the molecule into smaller new compounds. The spectrum of the pure 50 ppm Xylenol Orange Sodium Salt showed a maximum absorbance at 433 nm. Another minor peak was observed at 578nm. Without any other influences but LED light, the absorbance at the maximum peak of 50 ppm Xylenol Orange at 433 nm was decreasing slowly with time. Also, the absorbance of the peak at 578 nm increased gradually with time as shown in Fig 3.3 (a). Since no pH change was observed, the decrease in the absorbance at 433 nm could be due to the photodegradation of the dye, while forming an intermediate with a peak at 578 nm. Meanwhile, this change is too slow and could be enhanced via a suitable photocatalyst.

For the study of the photocatalysis using a photocatalyst under visible light radiation, two reactors with 25 ml of xylenol orange solution and 10 mg of the 10%TiO_2/Fe_3O_4 catalyst were covered and placed under LED while stirring for 3 days. The spectrum was recorded in triplicates, then the average was calculated then and plotted, as shown in Fig 3.3 (b) , and in Figure 3 and Figure 4 in the appendix. It was noticed that there is a change in the UV-Vis spectrum with time. The main peak of the dye was found to be at 433 nm. Another minimal peak was found at 578 nm. The absorbance at the main peak of the dye was decreasing. Meanwhile, the absorbance of the peak at 578 nm increased with time. The new peak at 578 nm suggests formation of new molecule with a purplish color which could be considered as an intermediate. Indeed, the pH of the medium was stable with time. Thus, the increase of absorbance at 578 nm has proved to be associated with forming a new product rather than a change in the pH of the medium.

No further peaks were observed, which implies the absence of complexation between iron ions that the catalyst consists of and Xylenol Orange dye. Complexation with Fe (II) and Fe (III) ions will result in a formation of new peaks at 475 nm and 585 nm respectively (98). A recent study conducted by Chrisnasari et al. have showed that such complexations between Xylenol Orange and iron oxides are usually indicated by the absence of an isosbestic point. Also, the obtained UV-Vis spectra for the complex have showed a major peak around 520 nm (99). Meanwhile, this contradicts with our results that was mentioned earlier, which proves that no metal complexation had resulted.

The last condition studied presence of the catalyst with absence of any sorts of radiation. Two reactors containing 25 ml of 50 ppm xylenol orange solution and 10 mg of the 10%TiO_2/Fe_3O_4 catalyst were covered and put in the dark for 3 days, the spectrum was recorded in triplicates, the average was calculated and plotted, as shown in Fig 3.3 (b), and Fig 5 and Fig 6 in the appendix. The same trend that was previously observed in the case of presence of light radiation was also observed in absence of light. An increase in absorbance at 433 nm, a decrease at 578 nm, and absence of complexation formation were observed. On the other hand, the change was slower than the one obtained under LED radiation. Hence, the catalyst had the ability to degrade the dye even in the dark without photon activation.

Figure 3.3

Absorbance of 50 ppm Xylenol Orange with time

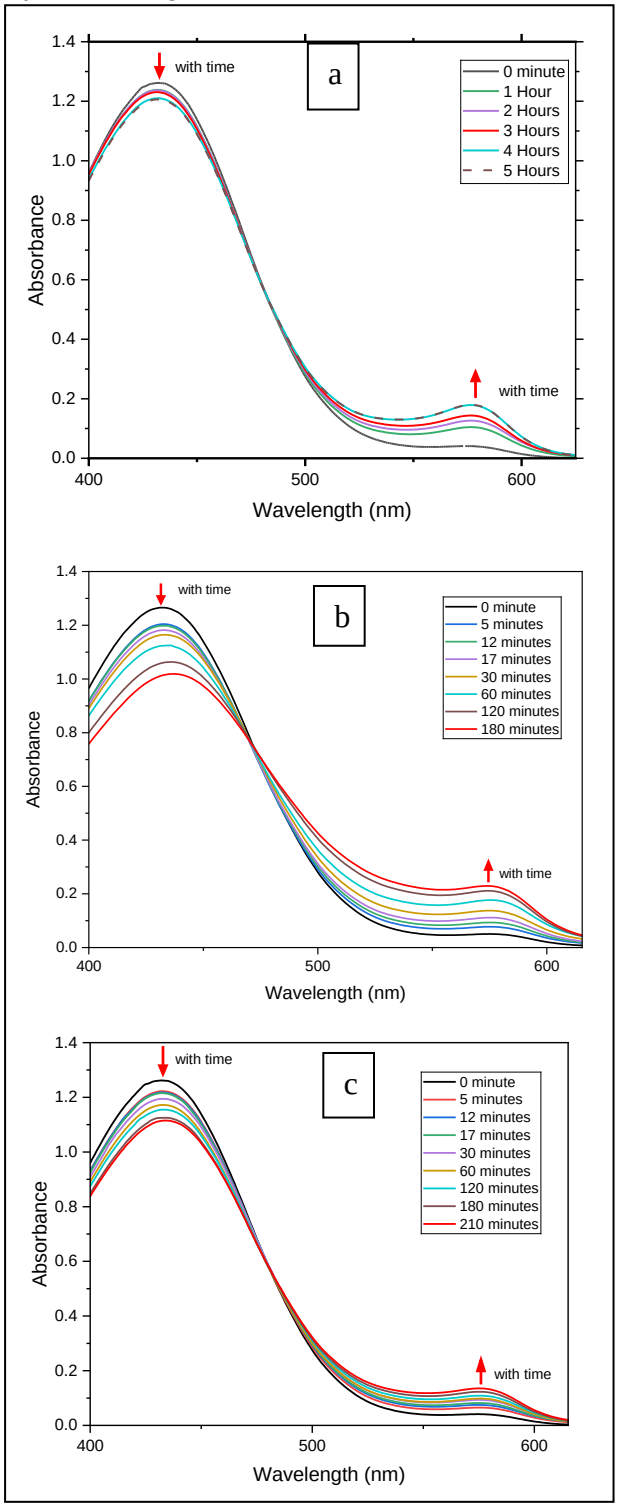

Not: (a) with no catalyst under LED radiation (b) first day of treatment with catalyst under LED radiation (c) in presence of catalyst in the dark.

In summary, both LED and the catalyst were influencing the photodegradation process positively.

3.2.2 Kinetic Study

Chemical Kinetics is the study of chemical reaction rates. It is essential in monitoring the progress of a reaction and predicting how fast a reaction would reach the equilibrium point. Reaction rates depend mostly on the initial concentrations of the reactants, and the concentration of the products in some cases(100).

The reaction rate is usually described by a proportional relationship to the rate constant with the n^{th} order if the initial concentration of the reactants. While the being independent from the initial concentrations of the reactants, the rate constant is dependent on the temperature (100).

By referring to the method of initial rates, and by considering an isolation of other influences, the rate of a reaction (υ) consists of one reactant only, or one reactant is in great excess on the other reactants, could be as described as the product of

multiplication the rate constant (k_r) and the concentration of the reactant [A] as shown below (100):

$$\upsilon = k_r[A]^n \qquad Eq.15$$

If n=1, the reaction is called first-order reaction and will have the following formula (100),

$$\upsilon = k_r[A] \qquad Eq.16$$

and this could be written in the integrated form in time (t) as (100):

$$ln\frac{[A]}{[A]_0} = -k_r t \qquad Eq.17$$

Since

$$ln\frac{[A]}{[A]_0} = ln\,[A] - ln\,[A]_0 \qquad Eq.18$$

equation (18) could be written as following (100):

$$ln[A] = -(k_r t + ln[A]_0) \quad \text{Eq.19}$$

If n=2 in equation (16), the reaction is called a second-order reaction and will have the following formula (100):

$$\upsilon = k_r[A]^2 \quad Eq.20$$

The integrated second law called be also written as (100):

$$\frac{1}{[A]} = k_r t + \frac{1}{[A]_0} \quad \text{Eq.21}$$

Meanwhile, the order of the reaction could be determined only by referring to data obtained from experimental work (100).

In our study, the experimental part was done using 25 ml of 50 ppm Xylenol Orange solution with pH of 5.5 added to 10 mg of 10%TiO_2/Fe_3O_4 catalyst. The sample was put in a closed plastic reactor and placed under LED radiation while stirring, and the spectrum was recorded in triplicates with time.

To determine the rate order of the photocatalysis reaction of Xylenol Orange at 433nm and forming the intermediate at 578nm representing, both inverse of the absorbance and ln absorbance were plotted versus time.

By referring to equations (19) and (21), a linear fit of plotting ln of absorbance versus time represents a first-order reaction. While a linear fit of plotting the inverse of the absorbance versus time represents a second-order reaction.

After neglecting the initial lag phase points, it was found that the linear fit for the first order plot had an R^2 of 0.977 as shown in Fig 7 (a) in the appendix. On the other hand, the second order plot had an R^2 =0.980 as illustrated in Fig 7 (b) in the appendix. Since the second order linear fit had a better R^2 than R^2 of the first order linear fit, the photocatalysis reaction is more probably following the second order laws.

Another two plots with the same strategy mentioned above were drawn to determine the rate order of forming the new intermediate at 578 nm. It was observed that the absorbance of the intermediate increases over time, though not in a perfectly linear manner. Additionally, the linear fits for both first- and second-order reaction plots

deviated from an ideal linear fit. Meanwhile, forming the intermediate is closer to the first order rate with R^2=0.966, as shown in Fig 7 (c) in the appendix, while R^2 for the second order linear fit was only 0.91 as shown in Fig 7 (d) in the appendix. This may be a result of a multi steps mechanism of forming the intermediate before being stable and recognized for absorbance at 578 nm. Also, it may be the case that part of the intermediate is breaking into smaller molecules, so the absorbance was found to fluctuate over time, showing both increases and decreases rather than following a consistent trend.

It should be considered that the reaction was in progress while reading the spectrum in triplicate, which result in some significant error bars due to the rapid change in concentration from the first reading to the second, which is affecting the absorbance value as well.

In conclusion, the photocatalysis of Xylenol Orange at absorbs 433nm follows the law of 2nd order reactions. Although the formation of the intermediate absorbing at 578 nm did not exhibit a perfectly linear relationship over time, the R^2 value suggests it is more likely following 1st order reaction kinetics.

3.2.3 Effect of Doping on the Photocatalytic Properties of TiO2

As mentioned early in section 1.7, the main goal of this study is to improve the photocatalytic properties of TiO_2. As a result, it is important to compare the results achieved from using pure TiO_2 to the one achieved from the synthesized 10%TiO_2/Fe_3O_4.

For this study, the effect of equal amounts of TiO_2 and 10%TiO_2/Fe_3O_4 on 25 ml of 50 ppm of Xylenol Orange solution with pH equal to 5.5 were studied under LED light while stirring. The first difference is that TiO_2 is diamagnetic, hence a stirrer bar was added to the reactor. As mentioned in section 3.1, the synthesized 10%TiO_2/Fe_3O_4 is paramagnetic, so no stirrer bar was needed. Another difference is that the synthesized catalyst does not dissolve in Xylenol Orange solution, so a strong magnet was sufficient to separate all of the magnetic nano particles and purify the medium post treatment. But the rutile TiO_2 had turbid the solution, so centrifugation was needed to purify the medium before recording the UV-Vis spectrum and post treatment as well.

It was noticed that the change in spectrum of Xylenol Orange in presence of rutile TiO_2 had the same trend, as shown in Fig 3.4 (a) as the change in spectrum of Xylenol Orange solution in presence of 10% TiO_2/Fe_3O_4 as illustrated in Fig 3.3 (b). The absorbance of the main peak of Xylenol Orange at 433 nm decreased, the peak at 578 nm increased with time. No other significant peaks were observed.

For more precise comparison, percent change in absorbance for both peaks at 433nm and 578nm representing the removal of the dye and forming the intermediate respectively were calculated along with their errors, as shown in Fig 3.4 (b) and Fig 3.4 (c).

$$\%change = \frac{Abs_{initial} - Abs_{final}}{|Abs_{inital}|} \times 100\% \qquad \text{Eq.22}$$

During the first 30 minutes of the treatment, both TiO_2 and 10%TiO_2/Fe_3O_4 had the same percent change in absorbance at 433nm. After 1 hour of treatment under LED, it was noticed that the decrease in absorbance at 433nm started to be more rapid in presence of TiO_2 than the decrease in presence of the synthesized catalyst of TiO_2 and 10%TiO_2/Fe_3O_4. Even though the experiment was done in duplicate, and the spectra recorded in triplicate. The resulted errors were negligible, which indicates the high accuracy of the experiment.

The change at 578nm was also found to be more rapid in presence of TiO_2 than in presence of 10%TiO_2/Fe_3O_4. Indeed, the difference is not significant in most readings. Also, the error bars correspond to the change at 578nm are considered to be significant. One explanation could be that the reaction of forming the intermediate was not stable and changing rapidly from one reading to another.

Since it was noticed that the significant difference in degrading the peak at 433nm did not result a significant increase of absorbance at 578nm in presence of rutile TiO_2, this could be either a result of TiO_2 working as adsorbent, or due to breaking the intermediate into smaller compounds.

It could be stated that 10%TiO_2/Fe_3O_4 is working as a photocatalyst with a reliable efficiency to TiO_2. Moreover, it is easier to separate it from the medium after the treatment. In brief, doping TiO_2 with the paramagnetic nano particles of Fe_3O_4 preserves the photocatalytic properties of TiO_2, while enhancing the post treatment purification method.

Figure 3.4

Effect of rutile TiO_2 with time on 50 ppm Xylenol Orange solution

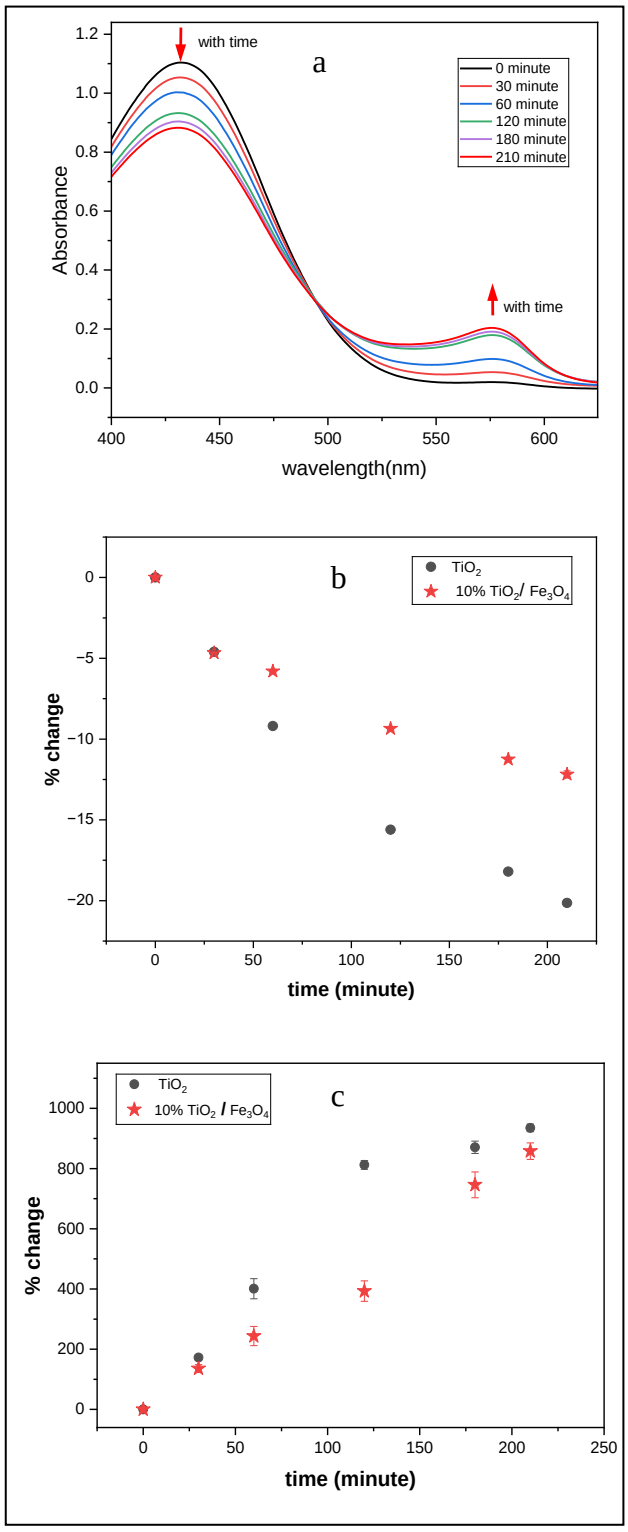

Not: (a) full spectrum with time, (b) percent change in absorbance compared to 10%TiO2/Fe3O4 at 433nm, (c) percent change in absorbance compared to 10%TiO2/Fe3O4 at 578nm.

In summary, the synthesized photocatalyst of 10%TiO_2/Fe_3O_4 showed a reliable photocatalytic efficiency compared to rutile TiO_2. Meanwhile, post treatment purification is easier in the case of using the synthesized catalyst.

3.2.4 Effect of Doping on the Photocatalytic Properties of Fe3O4

Preparation of 10%TiO_2/Fe_3O_4 cost additional reagents than synthesizing Fe_3O_4 alone. Also, Fe_3O_4 by itself is a para magnetic semiconductor with small band gap and easy to purify (101). Hence, it is important to study the doping effect on Fe_3O_4 nano particles.

In this study, the effect of equal amounts of Fe_3O_4 and 10%TiO_2/Fe_3O_4 on 25 ml of 50 ppm of Xylenol Orange solution with pH equal to 5.5 were studied under LED light while stirring. Both catalysts are paramagnetic and have magnetic properties. Hence, a strong magnet was efficiently used to purify the treated solutions after treatment. In terms of purification methods, both catalysts have the same simplicity.

The spectrum of both conditions was plotted with time. The plot of absorbance in presence of 10%TiO_2/Fe_3O_4 had the same trend discussed before and shown in Fig 3.3 (b), it showed a decrease in the absorbance at 433nm and increase at 578 nm. Also, the changes in Xylenol Orange spectrum in presence of Fe_3O_4 showed that the absorption is decreasing at 433 nm and increasing near 578 nm without forming a clear peak at 578 nm, see Fig 3.5. In other words, the peak corresponding to the intermediate was not significant. In addition, the absence of an isosbestic point was noticed in the plot in presence of Fe_3O_4, as illustrated in Fig.3.5. As stated by Chrisnasari et al. an increase in absorbance at the range of (520-590) nm indicates the formation of Fe^{+3} -Xylenol Orange complex. These results indicate the formation of Fe-Xylenol Orange complexes rather than degradation (98, 99). Hence, the magnetic Fe_3O_4 nano particles did not work as photocatalyst, but rather Xylenol orange worked as metal indicator and formed a complex with iron ions. Therefore, attaching TiO_2 to Fe_3O_4 is very important, otherwise the magnetic nano particles will not work as a photocatalyst. In other words, it was confirmed that doping the nano particles of Fe_3O_4 enhances their photocatalytic properties.

Figure 3.5

Absorbance versus time of 25 ml of 50 ppm Xylenol Orange solution in presence of 10 mg Fe_3O_4.

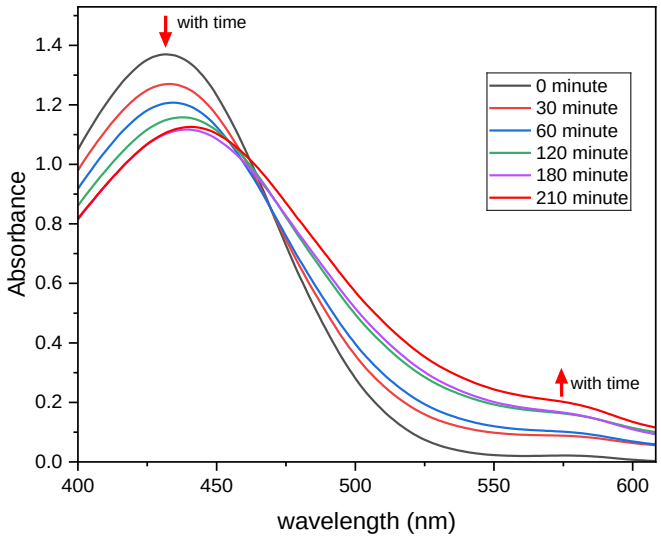

3.2.5 Effect of Amount of The Catalyst

Different amounts of photocatalyst lead to different photocatalysis efficiency. More catalyst means additional cost. Also, using too much catalyst may result in an adsorption treatment besides the photocatalysis.

While all conditions are fixed but the amount of photocatalyst, the effect of different amounts of 10%TiO_2/Fe_3O_4 was studied. As shown in Fig 8 in the appendix, the percent change in absorbance at both 433 nm and 578 nm were calculated along with their errors for all samples.

It was observed that increasing the amount of photocatalyst used improves the removal of Xylenol Orange, as indicated by a more pronounced decrease in the dye's main peak at 433 nm, see Fig 8 (a) in the appendix. This is a result of an increase in the surface area of the catalyst that interacts with the dye. Also, it was found that LED radiation enhances the removal of the dye in most cases.

On the other hand, increasing the amount of the catalyst beyond 10 mg had lowered the efficiency of forming the intermediate that is used to be forming at 578nm, see Fig 8 (b) in the appendix. This may be a result of an adsorption process that is occurring due increasing the amount of photocatalysts. By referring to Fig 3.3 (b), it was demonstrated that the intermediate keep increasing with time under radiation, without recording any

decrease in the absorbance at 578nm. Therefore, the decrease in absorbance with increasing amounts of photocatalyst cannot be attributed to the intermediate breaking down into smaller molecules. In other words, it may be the case that the increasing the surface area favored the adsorption on photocatalysis rather than degradation. Hence, it may be the case that increasing the amount of the photocatalyst enhances the removal of Xylenol Orange by both photocatalysis and adsorption. These results agree with the work of Zhang et al., they have observed that using excess loads of the photocatalyst may result in a light blockage. Accordingly, the photocatalysis efficiency will decrease (77).

In conclusion, increasing the amount of photocatalyst beyond 10 mg per 25 ml of Xylenol Orange is lowering the photocatalysis of the dye, and allowing adsorption to occur due to light blockage.

3.2.6 Effect of Solution's pH

The pH of the medium affects the surface of the photocatalyst which affects the interaction between photocatalyst and the dye (75). As discussed in section 1.6.1, increasing the pH increases the formation of $HO^{\bullet}$, but this is not the case for all photocatalysis mediums. The optimal pH is unique for each photocatalysis system depends on both the photocatalyst and the pollutant (80). As mentioned earlier, the only fixed rule is to choose a pH that is far from the PZC of the catalyst, which was found to be equal 4.69.

In this study, the photocatalysis was analyzed at four different pHs. At pH of 3.3, 5.55, 7.20, and 10.05. Acetic acid was used to adjust the pH of the solution to reach 3.3, and the solution has a fixed pH throughout the treatment. In normal conditions, Xylenol Orange is acidic with a stable pH ~5.5. The solution with adjusted pH of 7.20 using ammonia solution also had a stable pH thought the experiment. Ammonia solution was considered in obtaining a pH of 9.20, but the pH was not stable and dropped quickly to a lower pH equal 8.12. Hence, the solution was not considered in further analysis. Therefore, ammonia buffer solution was used at pH of 10 to make it more stable. Unfortunately, the pH decreases significantly during the treatment for both the pure solution and the one containing the photocatalyst.

The recorded spectra of the duplicate samples were recorded in triplets and averaged. It was noticed that the maximum absorbance for pure Xylenol Orange was at 433 nm in acidic and neutral condition, while it was at 578nm in basic conditions. The percent change in the absorbance of the Xylenol Orange peak at 433 nm and 578 nm were calculated for all samples along with the errors.

It was noticed that the decrease in the 433 nm increases with increasing the acidity of the medium, also the decrease in absorbance in absence of photocatalyst in the dark and under LED radiation is minor, see Fig 3.8 (a). Both LED and dark conditions in presence of the photocatalyst for neutral and acidic mediums are favorable. On the other hand, it was noticed that the pH of 10 is not stable for Xylenol Orange. The pH of the solution kept decreasing rapidly with time and resulted in a significant error in the spectrum readings. As a result, the absorbance at 433 nm is increasing with time rather decreasing, since lowering the pH of Xylenol Orange increases the absorbance at 433nm. In other words, the change of absorbance is due to the change in the pH of the medium.

For the change in absorbance at 578nm, it was observed that both increasing the acidity of the medium and LED radiation enhance forming the intermediate at 578 nm, see Figure 3.8 (b). In both neutral and acidic conditions and when exposed to LED radiation with no catalyst, a minor increase in absorbance at 578 nm was observed. Meanwhile, absorbance at 578 nm in the neutral conditions is not stable and may be mixed with the formed intermediate. Also, it could be the case that adsorption was occurring in neutral conditions. As mentioned above, the pH in the basic conditions were unstable, increasing the acidity lowers the absorbance at 578 nm rather than increasing it. Also, an intermediate may be formed. These two contrary results are mixed together resulting in a misleading result at the pH of 10.

Figure 3.6

Percent change of absorbance of Xylenol orange with different pH adjustments at: (a) 433 nm, (b) 578nm.

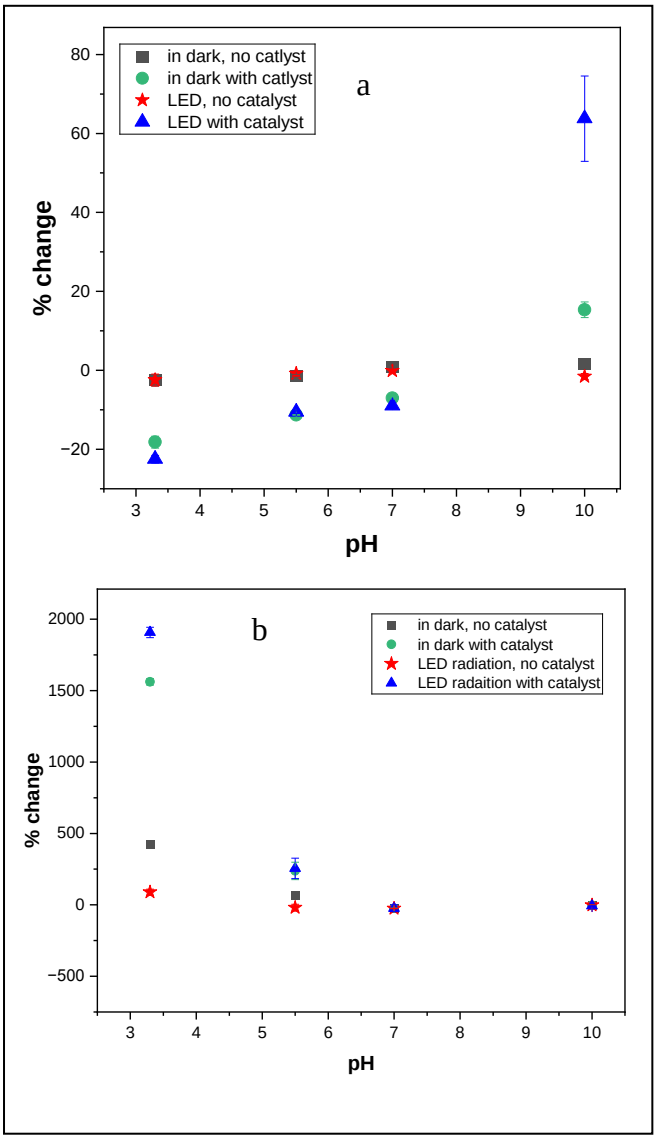

To summarize, the neutral and basic conditions result in misleading results. Therefore, acidic conditions are favored. Also, increasing the acidity and presence of light enhances the photocatalysis results.

3.2.7 Effect of Concentration of Xylenol Orange

Studying photocatalysis over a wide range of concentrations of Xylenol Orange is very important. High concentrated solutions may prevent photons of light from reaching the photocatalyst's surface. Also, low concentrated solutions may not interact efficiently with the photocatalyst.

In this study, different dilution factors were applied to a 100 ppm Xylenol Orange stock solution. For all concentrations, equal amount of photocatalyst were added to equal volumes of the different Xylenol Orange solutions. Then, percent change in absorption at both 433nm and 578nm were calculated along with their errors, see Fig 9 in the appendix.

In absence of catalyst but LED, it was noticed that the percent change at 433 nm was the same for all concentrations. In presence of the photocatalyst and LED radiation, the percent change was the greatest for the 10-ppm sample, but no clear relation was stated between the concentration of Xylenol Orange and the percent change of absorption at 433 nm, in both dark and LED radiation conditions, as shown in Fig 9 (a) in the appendix. Meanwhile, the presence of photocatalyst enhances the dye removal more than exposure to light alone.

In the absence of photocatalyst but with LED radiation, all concentrations had almost the same percent change at 578nm. Also, while addition of the photocatalyst but put in the dark, all concentrations had approximately the same percent of change. Additionally, there was no clear relationship between the percent change at 578 nm and concentration of Xylenol Orange solution in presence of photocatalyst under LED. Meanwhile, for each concentration, the maximum percent change was noticed in samples containing 10%TiO_2/Fe_3O_4 photocatalyst while being under LED radiation, see Fig 9 (b) in the appendix. Meanwhile, the latter samples had significant error bars. This may be due to recording the samples in triplicate while the reaction of forming the intermediate is not at equilibrium and increasing with time.

In other words, the concentration of Xylenol Orange has no direct effect on efficiency of photocatalysis. Moreover, the synthesized 10%TiO_2/Fe_3O_4 has performed a stable efficiency across a moderate range of dye's concentration. As a result, the synthesized photocatalyst could be used to purify water from Xylenol Orange in both concentrated and diluted media.

3.2.8 Effect of H_2O_2

As explained previously in section 1.6.1, adding oxidizing agents such as H_2O_2 increases the efficiency of photocatalysis, since it enhances the production of the active hydroxyl radicals. In this study, the effect of adding different concentrations of H_2O_2 was studied. This effect was studied using a 50 ppm of Xylenol Orange solution with pH =5.65. After averaging the absorbance recorded in triplicates, the percent change of peaks at 433 nm and 578 nm for all samples were plotted along with their errors, as shown in Fig.3.10.

It was noticed that the decrease in the absorbance at 433 nm is increasing with time in all samples and maximized in presence of 3%H_2O_2, see Fig 3.10 (a). Since all analyzed samples contained the same amount of the photocatalyst and the same concentration of Xylenol Orange, the enhancement of removing the dye is due to the enhancement of photocatalysis process only. In other words, there are no conditions that may favor a side adsorption process. On the other hand, the photocatalytic efficiency in absence of H_2O_2 was found to be higher than in presence of 1% H_2O_2 in all cases, and higher than in presence of 2% H_2O_2 at 2 hours of treatment. As mentioned earlier in equations (7) and (8), peroxide may start consuming the active hydroxyl radicals and producing non active species in addition to water molecules. Moreover, the positive holes on the catalyst's surface may react with the peroxide forming non-reactive species as the following equation shows(81):

$$TiO_2(h^+) + H_2O_2 \rightarrow TiO_2 + 2H^+ + O_2 \qquad Eq.23$$

Besides, it was noticed that the change in absorbance at 578 nm maximized with time in absence of H_2O_2. In the presence of H_2O_2, the change was unstable; the change was switching from an increase to a decrease and vice versa with time, see Fig.3.10 (b). In other words, the intermediate was both forming and degrading with time.

After 3 hours of treatment, the sample containing 3% H_2O_2 had the lowest absorbance at 578nm. Also, the removal of Xylenol Orange at 433 nm was at the maximum in presence of 3%H_2O_2. Hence, it was concluded that increasing the amount of oxidizing agent used increases the degradation of Xylenol Orange. Also, further degradation of the intermediate was observed. Meanwhile, such degradation of the intermediate was not observed in absence of H_2O_2. The photocatalyst was limited to degradation of the

dye into the intermediate at 578nm, since the absorbance at 578nm was always increasing with time. In other words, the addition of peroxide allowed a full degradation beyond forming an intermediate. It should be noted that the formed intermediate will be discussed in detail by referring to the obtained GCMS results.

To summarize, adding 3% peroxide enhances the photocatalytic efficiency of Xylenol Orange by 10%TiO_2/Fe_3O_4. Moreover, the degradation exceeds forming an intermediate, so the intermediate continues degrading into smaller molecules reaching a full degradation state.

Figure 3.7

The percent change in absorption of Xylenol Orange in presence of different concentrations of H_2O_2 at: (a) 433 nm (b) 578 nm

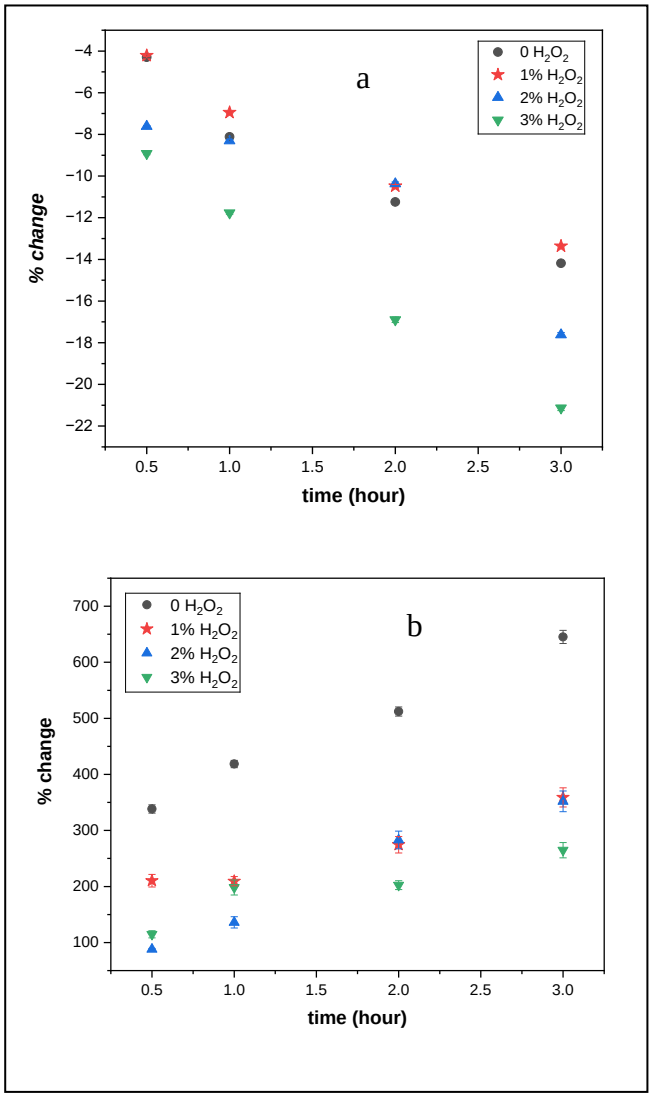

3.2.9 Optimal Conditions

An additional experiment was held under the optimal conditions that were determined in the previous sections. Since the concentration of Xylenol Orange did not have a direct influence on the photocatalysis process, 20 ppm Xylenol Orange solution was chosen for this experiment, since it is considered as a moderate concentration. The pH of the solution was adjusted to be acidic ~3.0. 25 ml of the latter solution was added to only 10 mg of 10%TiO_2/Fe_3O_4 photocatalyst. Also, 1 ml of 3% H_2O_2 solution was added to the sample. The averaged spectrum was plotted as shown in Fig 3.11.

It was noticed that absorbance at 433nm was decreasing with time. A shift of the maximum peak was noticed to be around 460 nm while decreasing with time was noticed. The percentage removal of the dye at 433nm exceeded 53% in 5 hours of LED radiation. Also, the maximum of the peak indicating the intermediate was shifted to be at 564 nm. It was noticed that the peak of the intermediate was increasing with time until it reached a maximum in 60 minutes then started decreasing with time. In other words, the intermediate starts breaking into smaller molecules. The sample was kept in the dark for 48 hours and the spectrum was recorded again. The percentage removal increased to reach 93%.

Figure 3.8

UV-Vis Spectrum of 25 ml of 20 ppm Xylenol Orange with time at acidic conditions, 10 mg 10%TiO_2/Fe_3O_4 catalyst, and 1 ml of 3% H_2O_2.

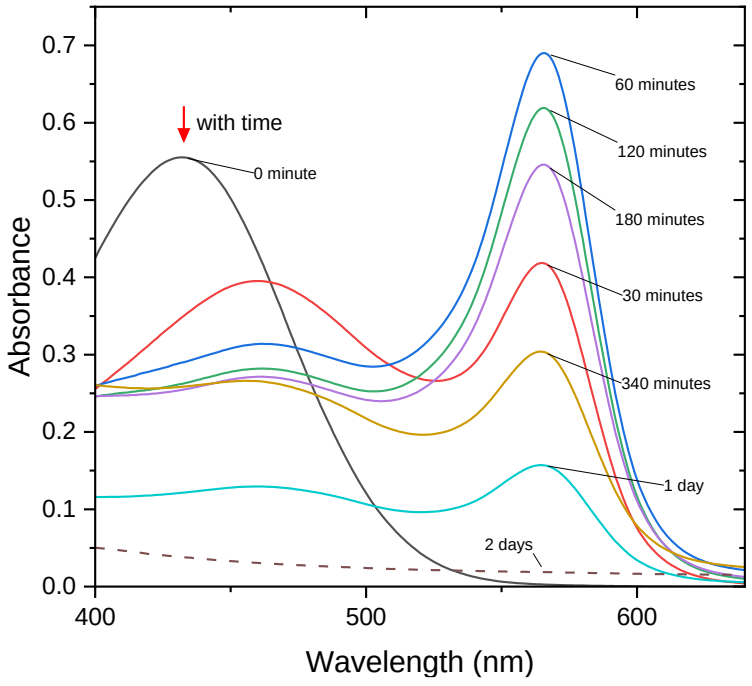

3.2.10 GC-MS Characterization

GC-MS chromatograms while using methanol as a mobile phase were obtained for a pure 20 ppm Xylenol Orange solution, and another treated solution of 25 ml of 20 ppm Xylenol Orange solution in presence of 10 mg 10%TiO_2/Fe_3O_4 catalyst and 1 ml of 3% H_2O_2 after 4 hours of LED radiation while stirring. The chromatograms were obtained respectively for the pure and treated samples as shown in Fig 3.12.

The obtained chromatograms by GCMS have successfully identified various distinctive peaks. Meanwhile, in both chromatograms, peaks with retention times of 2.18, 7.94, 8.7, 10.17, and 10.82 were identified by similarly research with NIST spectral library as impurities associated with the GC silica column. Therefore, they were disregarded in both chromatograms. In addition, in the chromatogram of pure Xylenol Orange in Fig 3.12 (a), methanol was also identified by similarly research with NIST spectral library at retention time of 2.045. Comparing the chromatogram of Xylenol Orange to the one after photocatalysis, a significant difference was noticed. In GCMS chromatogram of Xylenol Orange, peaks observed at retention times of 3.386, 4.259 ,4.491, 11.059, and 12.56 were identified by mass spectrum as large molecules, see Fig 3.12 (a). Meanwhile, these peaks were not observed in the chromatogram of the sample upon photocatalysis as shown in Fig 3.12 (b). Also, a was noticed.

Figure 3.9

GC-MS chromatograms in methanol for :(a) 20ppm pure Xylenol Orange solution, (b) 20 ppm Xylenol Orange solution upon photocatalysis in presence of 10%TiO_2/Fe_3O_4 and H_2O_2.

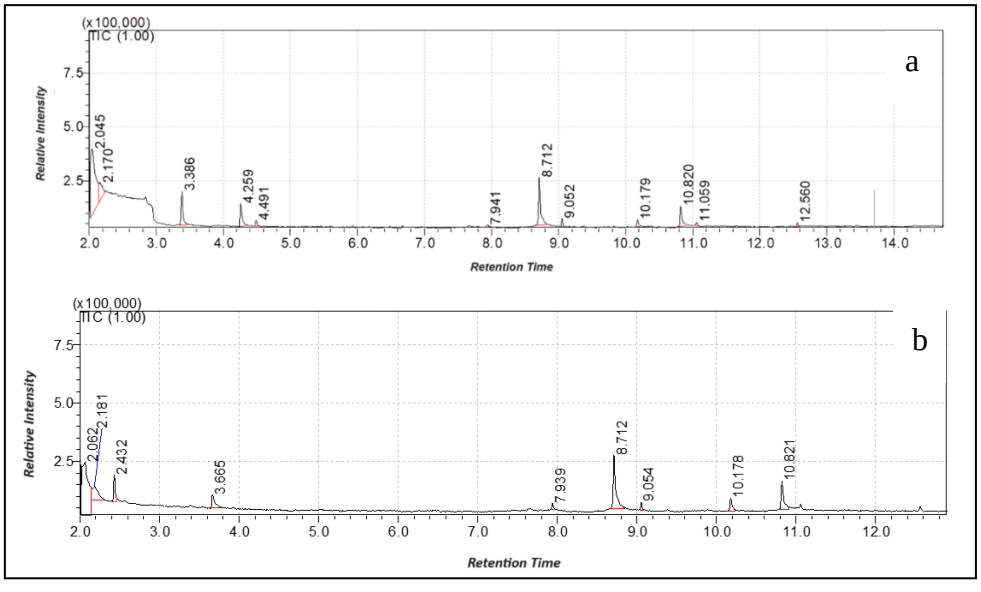

3.2.10.1 Mass Spectrum Analysis

The peak appears at a retention time of 2.432 mins in the chromatogram of the treated sample was suggested to refer acetic acid ($C_2H_4O_2$) peak. This investigation was done by referring to the mass spectrum library connected to the mass detector, which confirmed a 99% similarity score between the mass spectrum of the detected peak and the theoretical acetic acid's mass spectrum. Meanwhile, the peak area of acetic acid was found to represent 10.8% of the total areas of the identified peaks upon treatment.

For further illustration, the mass spectrum detected by the GC mass detector , Fig 10 (a) in the appendix, was compared to the experimental mass spectrum of acetic acid provided in NIST webbook (102), as shown in Fig 10 (b) in the appendix. Both spectra had a parent peak at 60 m/z which represents the molecular ion peak of acetic acid, since its molecular weight is equal to 60g/mol. Also, both spectra had fragments with significant relative intensity at 29 m/z correspondence for $[HCO]^+$ fragment, at 43 m/z representing the fragment of $[CH_3CO]^+$, and at 45 m/z for $[COOH]^+$ fragment. Also, it should be noted that the minor changes in both fragmentations and their relative intensities are due to contamination with methanol, which is the solvent for GC analysis. Also, a minor difference among the mass spectrum is associated with using different instruments which will result in different fragmentation. In conclusion, 10.8% percent of the compounds present upon photocatalysis of Xylenol Orange by 10%TiO_2/Fe_3O_4 and H_2O_2 consists of acetic acid.

In addition, the GC chromatogram for the treated Xylenol Orange sample showed a distinctive peak at retention time of 2.062 mins, see Fig 3.9 (b). Meanwhile, the latter peak was not recognized in the GC chromatogram of the pure sample in Fig 3.9 (a). Also, it was mentioned in the previous sections that the increase in absorbance at 578 nm in the UV-Vis spectra of Xylenol Orange upon treatment is associated with forming an intermediate. Hence, it was concluded that GCMS peak at retention time of 2.062 mins corresponds to the intermediate forming upon photocatalysis.

For further analysis, the chromatogram before this peak was subtracted for better analysis to reduce methanol contamination effects, then mass spectrum was analyzed, Fig 11 (a) in the appendix. According to similarity research, and by referring to the mass spectrum library connected with the GC mass detector, the search suggested a 76%

similarity match with 2-Hydroxyacetohydrazide ($C_2H_6N_2O_2$) which having a molar mass of 90 g/mol as a possible compound matching the experimental mass spectrum. Meanwhile, it is not possible to form this compound by photocatalysis of Xylenol Orange. Hence, further analysis was needed.

By referring to Xylenol Orange dye and investigating the possible bond breaking may occur due to the active hydroxyl radicals, it was suggested that Glycine molecules ($C_2H_5NO_2$) with molecular weight of 75g/mol could be formed as a result of breaking a C-N bond. By comparing both mass spectra recorded by GC mass detector Fig 11(a) and provided by NIST webbook for glycine (103), Fig 11 (b) in the appendix. It was noticed that both have a base peak at 30m/z, 31m/z, 45m/z, and 75m/z. The 75m/z fragment is considered as the molecular ion peak. The peak at 30m/z represents the fragment formed while losing a carboxylic acid group and forming $[CH_2NH_2]^+$, the peak at 31m/z correspondence to C-N cleavage and forming $[CH_3O]^+$ fragment, the peak at 45m/z is due to $[CH_2NH_2CO]^+$ fragment. Meanwhile, the relative intensities for the different fragments in general are not the same in both spectra. For example, the relative intensity for the fragment at 75m/z is higher than the relative intensity of the fragment at 30m/z in experimental mass spectrum, meanwhile the opposite was observed in the mass spectrum provided by NIST. This is a possible result of methanol contamination.

Methanol (CH_4O) has a molecular weight of 32g/mole. Its mass spectrum has a significant molecular ion peak at 32 m/z , Fig 11 (c) in the appendix,(104). Also, a strong base peak appears at 31m/z due to a hydrogen atom loss to form the fragment of $[CH_3O]^+$. Further fragmentations were due to a loss of two hydrogens, this result in a strong base peak at 31m/z. Hence, the relative intensity at fragmentations of 32 m/z, 31m/z, and 30m/z in the mass spectrum of the intermediate formed by photocatalysis of Xylenol Orange will be higher than usual due to methanol contamination.

Iminodiacetic acid ($C_4H_7NO_4$) with molecular mass of 133g/mol is another possible compound to be considered as the intermediate forming at retention time of 2.062 mins upon photocatalysis of Xylenol Orange. As mentioned in chapter one, iminodiacetic acid is used in the synthesis of Xylenol Orange. Hence the spectrum provided by NIST (105), Fig 11 (d) in the appendix, was compared to the experimental detected by GC mass detector Fig 11 (a) in the appendix. Both spectra have a parent peak at 133 m/z

that refers to the molecular ion peak of iminodiacetic acid. Both spectra also have a base peak at 30m/z which corresponds to $[CH_2NH_2]^+$ fragment. There is also a base peak at 42m/z that is either for $[C_2H_4N]^+$ or $[CH_2CO]^+$ fragments. The peak at 70m/z in both spectra refers to a $[C_3H_4NO]^+$ fragment. The peak at 75m/z refers to glycine molecule, since glycine is part of the iminodiacetic acid structure. Meanwhile, the base peak at 114m/z in both spectra refers to the loss of hydroxyl group to form $[C_4H_6NO_3]^+$ fragment. Meanwhile, the relative intensities for the different fragments in general are not the same in both spectra, this may be a result of methanol and other impurities contamination.

In conclusion, the intermediate formed by photocatalysis of Xylenol Orange 10%TiO_2/Fe_3O_4 may be a mixture of both glycine and iminodiacetic acid. The impurities resulting from both the methanol as a solvent and the different compounds present in the photocatalysis medium.

3.2.11 DFT Calculations

Density functional theory is very helpful in confirming the optimized structures of the different molecules along with their UV-Visible spectra. It is also helpful in calculating their ground state energy. Thus, it was used to confirm both the structure of Xylenol Orange used in this study and the possible forming compounds upon photocatalysis.

3.2.11.1 TD-DFT Calculations

B3LYP functional with basis set of ma-def2-SVP with CPCM solation model were first used to optimize the expected structure of Xylenol Orange sodium salt mentioned earlier in Table 1.1. Then the TD-DFT for the first 24 excited states of the preoptimized structure were calculated and plotted as shown in Fig 12 in the appendix. The obtained UV-Vis spectrum in arbitrary units (a.u) showed a maximum peak in the visible region at 420nm. Also, a peak in the UV region was observed at 303nm. Meanwhile, the experimental maximum of Xylenol Orange Sodium salt was found earlier to be at 433nm. In addition, a peak in the UV region was observed at 273mn. As previously discussed by Dr. Badran et al. research, errors associated with optimization may result in minor differences between the calculated spectrum using TD-DFT and the experimental spectrum (106). While neglecting the minor difference in the maximum wavelength between both spectra, the similarity between the experimental and

theoretical UV-Vis confirmed the correct structure of the Xylenol Orange salt in this study.

To explore the excited states responsible for the main peaks in the UV-Vis spectra, further analysis for the TD-DFT output file was done. Several possible transitions were observed as pure singlet transitions with energy equal to 2.953 eV and an oscillator strength equal to 0.915 be responsible for the peak obtained in the visible region at 420nm. Meanwhile, the transition with the highest contribution was stated to be a transition from orbital 180a to 181a orbital. For better visualization of the orbitals, we have referred to the MO diagram obtained from Chem Craft as shown in Fig 13 in the appendix. It was noticed that all the possible transitions responsible for the peak in the visible region at 420 nm have resulted from transitions among the various HOMO's orbitals. Meanwhile, the transition between orbitals 180a and 181a is taking place from the HOMO-1 to the HOMO orbitals of Xylenol Orange.

Also, the contribution of three different excited states was observed to be responsible for the peak lays in the UV region at 303 nm. The first excited state correspondence to a transition among singlet states with energy equal to 4.05eV and oscillator strength equal to 0. 0229. The second excited state correspondence to a transition between singlet states with energy equal to 3.68 eV and oscillator strength equal 0.0358. Meanwhile, both transitions are taking place from the HOMO-9 to the HOMO orbitals of Xylenol Orange. The last excited state correspondence to a transition between singlet states with energy equal to 4.29 eV and oscillator strength equal to 0.229. This transition is taking place from the HOMO-1 to the LUMO orbitals of Xylenol Orange.

3.2.11.2 Bond Dissociation Energy Calculations

Bond dissociation energy calculation (BDE) is a very essential concept in chemistry, especially organic chemistry. It is defined as the change in enthalpy of a molecule upon breaking a chemical bond within it (107, 108) :

$$A - B \rightarrow A^{\bullet} + B^{\bullet} \qquad \text{Eq.24}$$

BDE values help in understanding the structure of the molecules, estimate the hardness and easiness of breaking a bond, and predict the changes may happen due to the molecules upon the different chemical reactions(107). The thermodynamic and kinetic

changes could be predicted through the values of BDE. Also, the possible mechanisms could be studied and confirmed through BDE (109).

In this study, the BDE of the different fragments that may be converted later to form the post treatment compounds discussed earlier which are acetic acid, glycine, and iminodiacetic acid will be calculated. BDE is usually studied in the gas phase (108), but photocatalysis was performed in aqueous media, hence, a CPCM (water) solvation model was used for the optimization with frequency calculations the different structures. Also, it should be noted that a simplified structure of Xylenol Orange salt was used to perform these calculations. This was to reduce both the computational and time cost associated with optimizing the huge molecule of Xylenol Orange dye. No major change in the calculated values is expected upon molecular simplification, since the excluded parts of the dye have no direct influence on the bonds considered to break.

Once the optimizations were done, the molecular energies in Hartree's were calculated using the formula:

$$Enthalpy = SPE + ZPE \qquad Eq.25$$

Table 3.1 lists the simplified molecule used for BDE calculations and the possible fragmentations to be formed along with their optimized structures and their molecular energies in Hartree's.

Table 3.1

Molecular structures of the simplified Xylenol Orange and the possible fragmentations

Name	Molecular Formula	Molecular structure	Enthalpy at 0K (Hartree/mol)
Simplified Xylenol Orange structure	$C_{13}NH_{17}O_5$	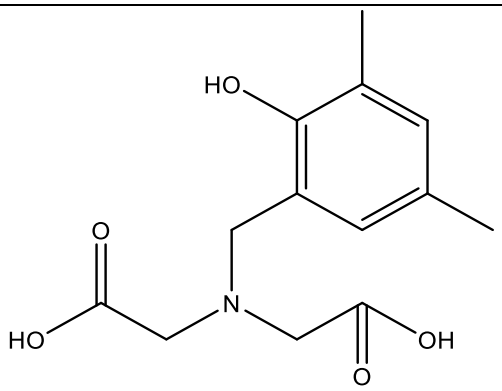	-935.09
Fragment A	$C_9H_{11}O$	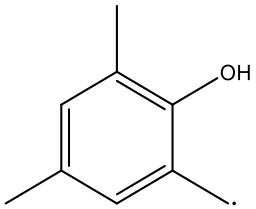	-424.05
Fragment B	$C_4H_6NO_4$	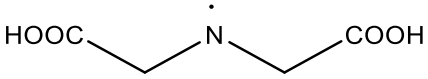	-510.96
Fragment C	$C_{11}H_{14}NO_3$	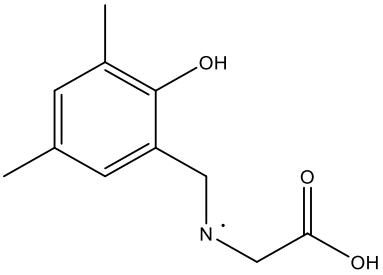	-706.88
Fragment D	$C_2H_3O_2$	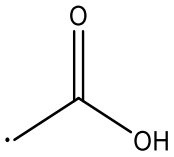	-228.13
Fragment E	$C_2NH_3O_2$	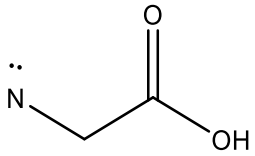	-282.74

BDE was calculated as the enthalpy change using the equation below:

$$BDE = (E_{products} - E_{reactants}) \qquad Eq.26$$

Since the obtained energy values generated by Orca were in Hartree/mol, multiplying the obtained values by a constant equal to 2625.499622 was used to convert the energy units to kJ/mol.

The first BDE calculation was done for breaking the C-N bond in the simplified Xylenol Orange molecule to form fragments A and B. Fragment B is then converted to form iminodiacetic acid. In other words, the first calculated BDE refers to forming iminodiacetic acid which was discussed earlier as a possible intermated formed upon photocatalysis. The second and third BDE calculations are associated with forming acetic acid. The first pathway of forming acetic acid is by directly breaking the C-N bond in the simplified Xylenol Orange molecules to form fragments C and D, then fragment D is converted directly to form acetic acid by bonding with a hydrogen. The second pathway to form acetic acid is by breaking the C-N bond in fragment B to get fragments C and E, which will be converted to acetic acid and glycine, respectively, by bonding with a hydrogen atom. Table 3.2 Summarize these results.

Table 3.2

BDE calculations for possible fragmentations of Xylenol Orange

Starting Molecule	Resulted fragments	Calculated BDE (kJ/mol)
Simplified Xylenol Orange	A, B	226.7
Simplified Xylenol Orange	C, D	207.7
Fragment B	D, E	218.0

3.3 Catalyst Recovery and Reuse

Reusable catalysts are favorable. They are considered economical and environmentally friendly. Easy recovery, minimal damage during the experiment, multi chemical stability, and the ability to multi reuse cycles enhance the features of the photocatalyst.

In our study, the magnetic nano particles of 10%TiO_2/Fe_3O_4 were extracted from the aqueous mediums of treatment by strong magnet. The magnetic features were preserved post photocatalysis treatment. Three different solutions were used to wash the catalyst to reduce catalyst poisoning. One part of the catalyst was washed with 2mM NaOH, the second with 2mM HNO_3, and the third with ethanol. Low concentrated acid and base were used to prevent any damage to the active sites of the catalyst. Also, ethanol was

used as an organic solvent that helps in removing organic impurities. Indeed, it is the same solvent used in synthesizing the photocatalyst.

The choice of operating the reuse experiments at the optimal conditions was made to obtain the highest efficiency at each cycle. After recording the spectrum post treatments, percent removal at 433 nm in all cases were calculated and plotted along with errors as shown Figure 3.10 (a). Compared to the fresh catalyst, which had a removal efficiency of 54%, washing with ethanol achieved the highest efficiency among the treatments, reaching 40.9%. In contrast, washing with NaOH reduced the removal efficiency to 37.6%, while washing with HNO_3 showed moderate results with 27.9% removal. In all instances, it was observed that the catalyst could be reused across multiple cycles.

Since the ethanol gave the highest efficiency, the catalyst was extracted another time to be used in more reuse cycles. Applying optimal conditions again, the catalyst was subjected to another two cycles of reuse. Percent removal was calculated and plotted as shown in Fig.3.10 (b). It was observed that the catalyst maintains reliable efficiency even after three cycles of reuse, with the percent removal decreasing to 29% by the third cycle.

Figure 3.10

Efficiency of the reused catalyst in 4 hours: (a) at different washing solutions, (b) at different number of cycles

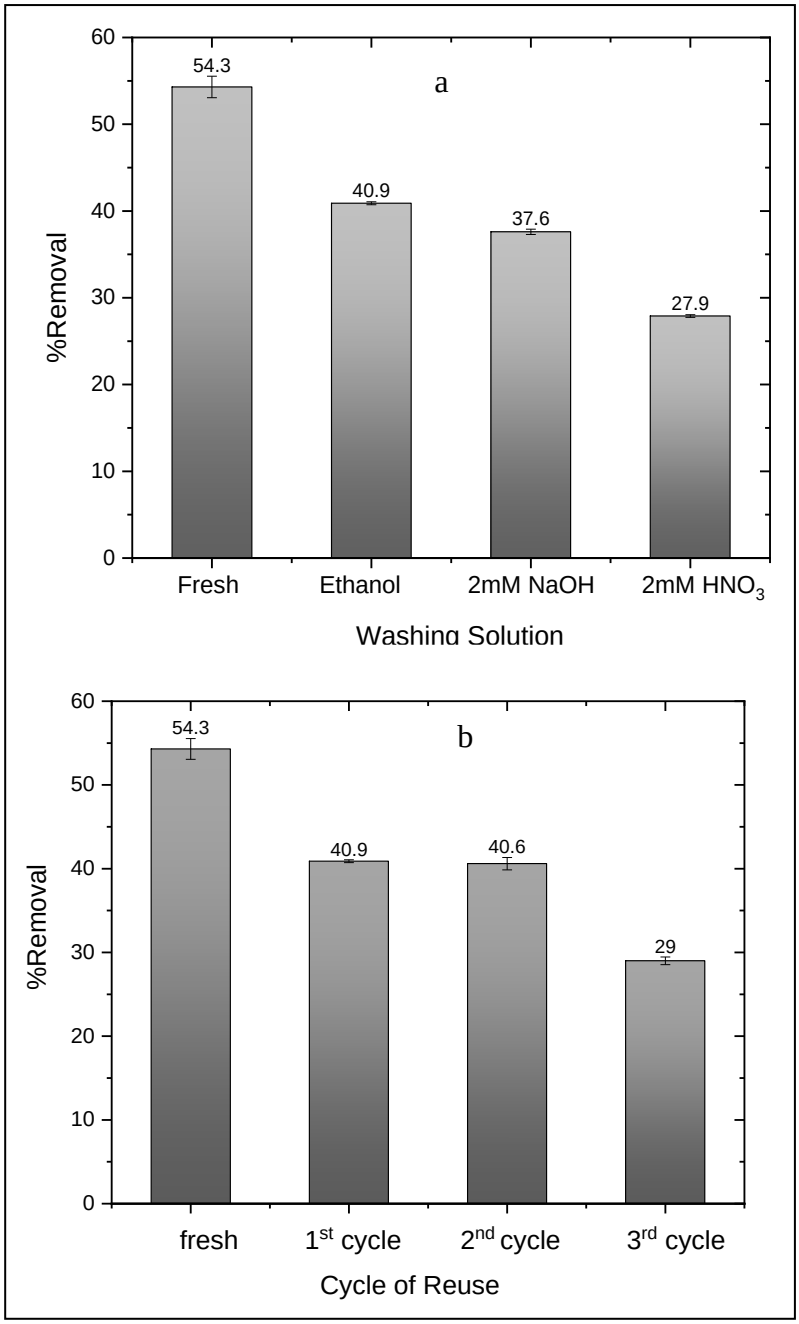

In conclusion, the magnetic nano particles of 10%TiO_2/Fe_3O_4 could be easily extracted post treatment and be reused for another 3 cycles of photocatalysis will keeping a reliable efficiency compared to the efficiency of the fresh photocatalyst.

3.4 Conclusion

In this study, doping TiO_2 with the para magnetic Fe_3O_4 magnetic nano particles was successfully carried to obtain 10%TiO_2/Fe_3O_4. The resulting nano particles were proven to preserve the photocatalytic efficiency of TiO_2 under visible light radiation, while the successful doping with para magnetic nanoparticles has enhanced the post treatment purification technique. Due to the small band gap of Fe_3O_4, the nanoparticles have showed a moderate photocatalytic efficiency in the dark. It was observed that the photocatalysis efficiency is independent of the concentration of Xylenol Orange solution and decreases with increasing the amount of 10%TiO_2/Fe_3O_4. Meanwhile, full degradation of Xylenol Orange was achieved in acidic conditions and in presence of H_2O_2. A kinetic study was conducted proving that the degradation increases with time, and the reaction follows the second order rate. The synthesized nano particles were found to be recoverable by washing with ethanol while preserving a moderate photocatalytic efficiency for at least three cycles of reuse. Briefly, the synthesized para magnetic nano particles of 10%TiO_2/Fe_3O_4 could be used as a photocatalyst reaching a full degradation under visible light radiation while being both economically and environmentally friendly.

3.5 Recommendations

This study was designed to fit the laboratory scale. Meanwhile, there are several suggestions that could be studied in the future to improve this work:

1. Upgrade the use of 10%TiO_2/Fe_3O_4 as a photocatalyst for Xylenol Orange to be applied on larger scales, industrial scale and wastewater treatment.
2. Examine the photocatalytic properties of the synthesized 10%TiO_2/Fe_3O_4 on other organic dyes and pharmaceutical drugs.
3. Try different light sources with different intensities and energies to test their effect on photocatalysis efficiency.
4. Study the effect of different doping percentages by mass of TiO_2 with Fe_3O_4
5. Investigate more on recovery techniques and try more washing solutions to enhance the reuse efficiency of the catalyst.

3.6 Limitations of The Study

1. The absence of instruments for Scanning Electron Microscopy (SEM) and X-ray Diffraction (XRD) at An-Najah National University laboratories prevents accurate characterization of the prepared 10%TiO_2/Fe_3O_4 .
2. Conducting a study to investigate the effects of changing TiO_2 percentage in the prepared photocatalyst was not possible due to the unavailability and difficulty in ordering $TiCl_3$.
3. The limited working hours of the laboratories prevented monitoring the reaction for more than 5 hours in a row.

List of Abbreviations

Abbreviation	Meaning
$[A]$	Concentration of compound A
$A^{\bullet}$	Radical of compound A
AFM	Atomic Force Microscopy
AOP	Advanced Oxidation Process
a.u	Arbitrary Units
BDE	Bond Dissociation Energy
BOD	Biological Oxygen Demand
CB	Conduction Band
CPCM	Conductor-like Polarizable Continuum Model
DFT	Density Functional Theory
e^-	electron
E_{bg}	Band Gap Energy
GC-MS	Gas Chromatography-Mass Spectrometry
$hole^+$	Positive charged hole
HOMO	Highest Occupied Molecular Orbital
kJ/mol	Kelo Joule Per Mole
k_r	Rate constant
LED	Light Emitting Diode
LUMO	Lowest Occupied Molecular Orbital
MO	Molecular Diagram
NIST	National Institute of Standards and Technology
PZC	Point of Zero Charge
R^2	Correlation Constant
SPE	Single Point Energy
t	Time
TD-DFT	Time Dependent Density Functional Theory
UNESCO	The United Nations Educational, Scientific and Cultural Organization
UV-Vis	Ultraviolet-Visible Spectroscopy
υ	Rate of the Reaction
VB	Valence Band
WQI	Water Quality Index
ZPE	Zero-point Energy

References

1. Pohorille A, Pratt LR. Is water the universal solvent for life? Origins of Life and Evolution of Biospheres. 2012;42:405-9.

2. Gray NF. Water Technology: An Introduction for Scientists and Engineers: Arnold; 1999.

3. Thomas C. Water in crisis: a guide to the world's fresh water resources. Oxford University Press; 1994.

4. Lin L, Yang H, Xu X. Effects of water pollution on human health and disease heterogeneity: a review. Frontiers in environmental science. 2022;10:880246.

5. Barakat R, editor Water in Palestine2013: Birzeit University, Ibrahim Abu-Lughod Institute of International Studies.

6. Daghara A, Al-Khatib IA, Al-Jabari M. Quality of drinking water from springs in palestine: West bank as a case study. Journal of Environmental and Public Health. 2019;2019(1):8631732.

7. Aliewi A, Al-Khatib IA. Hazard and risk assessment of pollution on the groundwater resources and residents' health of Salfit District, Palestine. Journal of Hydrology: Regional Studies. 2015;4:472-86.

8. Uddin Z, Ahmad F, Ullan T, Nawab Y, Ahmad S, Azam F, et al. Recent trends in water purification using electrospun nanofibrous membranes. International Journal of Environmental Science and Technology. 2022;19(9):9149-76.

9. Smith L. Historical perspectives on water purification. Chemistry and water: Elsevier; 2017. p. 421-68.

10. Mitiku A. Water pollution: Causes and prevention. Int J Pharm Sci Rev Res. 2020;60(2):94-101.

11. Singh MR, Gupta A. Water pollution-sources, effects and control. Centre for Biodiversity, Department of Botany, Nagaland University. 2016:1-16.

12. Tkaczyk A, Mitrowska K, Posyniak A. Synthetic organic dyes as contaminants of the aquatic environment and their implications for ecosystems: A review. Science of the total environment. 2020;717:137222.

13. Alegbe EO, Uthman TO. A review of history, properties, classification, applications and challenges of natural and synthetic dyes. Heliyon. 2024.

14. Benkhaya S, M'rabet S, El Harfi A. A review on classifications, recent synthesis and applications of textile dyes. Inorganic Chemistry Communications. 2020;115:107891.

15. Kiernan JA. Classification and naming of dyes, stains and fluorochromes. Biotechnic & histochemistry. 2001;76(5-6):261-78.

16. Gürses A, Açıkyıldız M, Güneş K, Gürses MS, Gürses A, Açıkyıldız M, et al. Dyes and pigments: their structure and properties. Dyes and pigments. 2016:13-29.

17. Dodgson N. What is the “opposite” of “blue”? The language of colour wheels. Journal of Perceptual Imaging. 2019;2:010401-1 to -12.

18. Sharma J, Sharma S, Soni V. Classification and impact of synthetic textile dyes on Aquatic Flora: A review. Regional Studies in Marine Science. 2021;45:101802.

19. Robinson T, McMullan G, Marchant R, Nigam P. Remediation of dyes in textile effluent: a critical review on current treatment technologies with a proposed alternative. Bioresource technology. 2001;77(3):247-55.

20. Cruz L, Basílio N, Mateus N, de Freitas V, Pina F. Natural and synthetic flavylium-based dyes: The chemistry behind the color. Chemical Reviews. 2021;122(1):1416-81.

21. Abe FR, Mendonça JN, Moraes LA, de Oliveira GA, Gravato C, Soares AM, et al. Toxicological and behavioral responses as a tool to assess the effects of natural and synthetic dyes on zebrafish early life. Chemosphere. 2017;178:282-90.

22. Barciela P, Perez-Vazquez A, Prieto M. Azo dyes in the food industry: Features, classification, toxicity, alternatives, and regulation. Food and Chemical Toxicology. 2023;178:113935.

23. Islam T, Repon MR, Islam T, Sarwar Z, Rahman MM. Impact of textile dyes on health and ecosystem: A review of structure, causes, and potential solutions. Environmental Science and Pollution Research. 2023;30(4):9207-42.

24. Wainwright M. The use of dyes in modern biomedicine. Biotechnic & Histochemistry. 2003;78(3-4):147-55.

25. Fried R, Oprea I, Fleck K, Rudroff F. Biogenic colourants in the textile industry–a promising and sustainable alternative to synthetic dyes. Green Chemistry. 2022;24(1):13-35.

26. Wainwright M. Dyes in the development of drugs and pharmaceuticals. Dyes and Pigments. 2008;76(3):582-9.

27. Sigurdson GT, Tang P, Giusti MM. Natural colorants: Food colorants from natural sources. Annual review of food science and technology. 2017;8(1):261-80.

28. Guerra E, Llompart M, Garcia-Jares C. Analysis of dyes in cosmetics: challenges and recent developments. Cosmetics. 2018;5(3):47.

29. Van der Schueren L, De Clerck K. The use of pH-indicator dyes for pH-sensitive textile materials. Textile research journal. 2010;80(7):590-603.

30. Belleza OJV, Villaraza AJL. Ion charge density governs selectivity in the formation of metal–Xylenol Orange (M–XO) complexes. Inorganic Chemistry Communications. 2014;47:87-92.

31. Nakayama H, Tachiyashiki S, Ishii M. Preparation of high purity xylenol orange and isolation of a new metallochromic dye by cation exchange column chromatography on SP-Sephadex. Analytical sciences. 1989;5(5):619-21.

32. Khan H, Tabassum S, Wahid M. Characterization of aqueous solution of cresol red as food irradiation dosimeter. Journal of radioanalytical and nuclear chemistry. 2009;280(3):635-41.

33. Summary for CID 60146744, Xylenol Orange sodium salt [Internet]. National Center for Biotechnology Information. 2024 [cited 27 July 2024]. Available from: https://pubchem.ncbi.nlm.nih.gov/compound/Xylenol-Orange-sodium-salt.

34. Alharthi FA, Al-Nafaei WS, Alshayiqi AA, Alanazi HS, Hasan I. Hydrothermal synthesis of bimetallic (Zn, Co) Co-doped tungstate nanocomposite with direct Z-scheme for enhanced photodegradation of xylenol orange. Catalysts. 2023;13(2):404.

35. Gay C, Collins J, Gebicki JM. Determination of iron in solutions with the ferric–xylenol orange complex. Analytical Biochemistry. 1999;273(2):143-8.

36. Elshan ND, Patek R, Vagner J, Mash EA. Spectrophotometric determination and removal of unchelated europium ions from solutions containing Eu-diethylenetriaminepentaacetic acid chelate–peptide conjugates. Analytical biochemistry. 2014;464:24-9.

37. Gonzalez Lopez M, Huteckova B, Lavicky J, Zezula N, Rakultsev V, Fridrichova V, et al. Spatiotemporal monitoring of hard tissue development reveals unknown features of tooth and bone development. Science Advances. 2023;9(31):eadi0482.

38. Saleem BA, Al-Qazzaz WA, Majeed SY. Determination of Indomethacin Derivative via Xylenol Orange Dye. Asian Journal of Water, Environment and Pollution. 2022;19(2):17-23.

39. Smith S, Boase N, Masters K, Hosokawa K, Asena A, Crowe S, et al. A very low diffusion Fricke gel dosimeter with functionalised xylenol orange-PVA (XOPVA). Physics in Medicine & Biology. 2019;64(20):205017.

40. Li N, Lin B, editors. Xylenol orange sorption on modified carboxymethyl cellulose. 2010 International Conference on Challenges in Environmental Science and Computer Engineering; 2010: IEEE.

41. Fa D, Miao Y. Hydrangea-like ZnS/$ZnIn_2S_4$ microspheres with outstanding photocatalytic degradation of xylenol orange and thymol blue under vis irradiation. Micro & Nano Letters. 2021;16(10):500-5.

42. Thomas AG, Syres KL. Adsorption of organic molecules on rutile TiO 2 and anatase TiO 2 single crystal surfaces. Chemical Society Reviews. 2012;41(11):4207-17.

43. Eshwar Rao S, Gayathri V. Poly (styrene–divinyl benzene)-immobilized Fe (III) complex of 1, 3-bis (benzimidazolyl) benzene: Efficient catalyst for the photocatalytic degradation of xylenol orange. Journal of Applied Polymer Science. 2018;135(29):46480.

44. Bhawani SA, Daud NAB, Bakhtiar S, Roland RM, Ibrahim MNM. Synthesis of molecularly imprinting polymers for the removal of Xylenol orange from water. Nature Environment and Pollution Technology. 2020;19(2):825-30.

45. Xiong XL, Shao CB. Removal of Xylenol Orange from Solutions by γ-Cyclodextrin-Grafted Carboxymethyl Cellulose. Advanced Materials Research. 2011;204:1180-3.

46. Uddin MG, Nash S, Olbert AI. A review of water quality index models and their use for assessing surface water quality. Ecological Indicators. 2021;122:107218.

47. Tyagi S, Sharma B, Singh P, Dobhal R. Water quality assessment in terms of water quality index. American Journal of water resources. 2013;1(3):34-8.

48. Kothari V, Vij S, Sharma S, Gupta N. Correlation of various water quality parameters and water quality index of districts of Uttarakhand. Environmental and Sustainability Indicators. 2021;9:100093.

49. Raman BV, Bouwmeester R, Mohan S. Fuzzy logic water quality index and importance of water quality parameters. Air, Soil and Water Research. 2009;2:ASWR. S2156.

50. Chidiac S, El Najjar P, Ouaini N, El Rayess Y, El Azzi D. A comprehensive review of water quality indices (WQIs): history, models, attempts and perspectives. Reviews in Environmental Science and Bio/Technology. 2023;22(2):349-95.

51. Marthinsen I, Sørgård T, editors. Zero discharge philosophy: a joint project between Norwegian authorities and industry. SPE International Conference and Exhibition on Health, Safety, Environment, and Sustainability?; 2002: SPE.

52. Zhang S, Wu Q, Ji H. Research on zero discharge treatment technology of mine wastewater. Energy Reports. 2022;8:275-80.

53. Koppol AP, Bagajewicz MJ, Dericks BJ, Savelski MJ. On zero water discharge solutions in the process industry. Advances in Environmental Research. 2004;8(2):151-71.

54. Nyabadza A, McCarthy É, Makhesana M, Heidarinassab S, Plouze A, Vazquez M, et al. A review of physical, chemical and biological synthesis methods of bimetallic nanoparticles and applications in sensing, water treatment, biomedicine, catalysis and hydrogen storage. Advances in Colloid and Interface Science. 2023:103010.

55. Sonune A, Ghate R. Developments in wastewater treatment methods. Desalination. 2004;167:55-63.

56. Ahmed S, Mofijur M, Nuzhat S, Chowdhury AT, Rafa N, Uddin MA, et al. Recent developments in physical, biological, chemical, and hybrid treatment techniques for removing emerging contaminants from wastewater. Journal of hazardous materials. 2021;416:125912.

57. Moosavi S, Lai CW, Gan S, Zamiri G, Akbarzadeh Pivehzhani O, Johan MR. Application of efficient magnetic particles and activated carbon for dye removal from wastewater. ACS omega. 2020;5(33):20684-97.

58. Bustos-Terrones Y, Rangel-Peraza JG, Sanhouse A, Bandala ER, Torres LG. Degradation of organic matter from wastewater using advanced primary treatment by O_3 and O_3/UV in a pilot plant. Physics and Chemistry of the Earth, Parts A/B/C. 2016;91:61-7.

59. Ahirrao S. Zero liquid discharge solutions. Industrial wastewater treatment, recycling and reuse. 489: Butterworth-Heinemann Oxford, UK; 2014.

60. Singh D, Singh D, Mishra V, Kushwaha J, Sengar M, Sinha S, et al. Strategies for biological treatment of waste water: A critical review. Journal of Cleaner Production. 2024:142266.

61. Saleh IA, Zouari N, Al-Ghouti MA. Removal of pesticides from water and wastewater: Chemical, physical and biological treatment approaches. Environmental Technology & Innovation. 2020;19:101026.

62. Kawan JA, Hasan HA, Suja F, Jaafar OB, Abd-Rahman R. A review on sewage treatment and polishing using moving bed bioreactor (MBBR). Journal of Engineering Science and Technology. 2016;11(8):1098-120.

63. Singh N, Nagpal G, Agrawal S. Water purification by using adsorbents: a review. Environmental technology & innovation. 2018;11:187-240.

64. Al-Tohamy R, Ali SS, Li F, Okasha KM, Mahmoud YA-G, Elsamahy T, et al. A critical review on the treatment of dye-containing wastewater: Ecotoxicological and health concerns of textile dyes and possible remediation approaches for environmental safety. Ecotoxicology and Environmental Safety. 2022;231:113160.

65. Oturan MA, Aaron J-J. Advanced oxidation processes in water/wastewater treatment: principles and applications. A review. Critical reviews in environmental science and technology. 2014;44(23):2577-641.

66. Salimi M, Esrafili A, Gholami M, Jonidi Jafari A, Rezaei Kalantary R, Farzadkia M, et al. Contaminants of emerging concern: a review of new approach in AOP technologies. Environmental monitoring and assessment. 2017;189:1-22.

67. Badran I, Manasrah A, Nassar N. A combined experimental and density functional theory study of metformin oxy-cracking for pharmaceutical wastewater treatment. . RSC Adv; 2019. p. 13403-13.

68. Groeneveld I, Kanelli M, Ariese F, van Bommel MR. Parameters that affect the photodegradation of dyes and pigments in solution and on substrate–An overview. Dyes and Pigments. 2023;210:110999.

69. Tome J, Gamelas SR, Lourenço L, Tomé A. Porphyrin-containing materials for photodegradation of organic pollutants in wastewaters. A review. Catalysis Science & Technology. 2024.

70. Snetkov P, Zakharova K, Morozkina S, Olekhnovich R, Uspenskaya M. Hyaluronic acid: The influence of molecular weight on structural, physical, physico-chemical, and degradable properties of biopolymer. Polymers. 2020;12(8):1800.

71. Karlsson JK, Woodford OJ, Al-Aqar R, Harriman A. Effects of temperature and concentration on the rate of photobleaching of Erythrosine in water. The Journal of Physical Chemistry A. 2017;121(45):8569-76.

72. Selvaraj V, Karthika TS, Mansiya C, Alagar M. An over review on recently developed techniques, mechanisms and intermediate involved in the advanced azo dye degradation for industrial applications. Journal of molecular structure. 2021;1224:129195.

73. Yang X, Chen Z, Zhao W, Liu C, Qian X, Zhang M, et al. Recent advances in photodegradation of antibiotic residues in water. Chemical Engineering Journal. 2021;405:126806.

74. Chen Q, Chen L, Qi J, Tong Y, Lv Y, Xu C, et al. Photocatalytic degradation of amoxicillin by carbon quantum dots modified K2Ti6O13 nanotubes: Effect of light wavelength. Chinese Chemical Letters. 2019;30(6):1214-8.

75. ZIELIŃSKA M, WOJNOWSKA-BARYŁA I, CYDZIK-KWIATKOWSKA A, ZIELIŃSKA M, WOJNOWSKA-BARYŁA I, CYDZIK-KWIATKOWSKA A. Physical and chemical treatment technologies for BPA removal from wastewater. Bisphenol A Removal From Water and Wastewater. 2019:29-60.

76. Rodrigues-Silva F, Santos CS, Marrero JA, Montes R, Quintana JB, Rodil R, et al. Continuous UV-C/H2O2 and UV-C/Chlorine applied to municipal secondary effluent and nanofiltration retentate: Removal of contaminants of emerging concern, ecotoxicity, and reuse potential. Chemosphere. 2024;361:142355.

77. Zhang D, Lv S, Luo Z. A study on the photocatalytic degradation performance of a [$KNbO_3$] 0.9-[BaNi 0.5 Nb 0.5 $O_{3-\delta}$] 0.1 perovskite. RSC advances. 2020;10(3):1275-80.

78. Hassaan MA, El-Nemr MA, Elkatory MR, Ragab S, Niculescu V-C, El Nemr A. Principles of photocatalysts and their different applications: a review. Topics in Current Chemistry. 2023;381(6):31.

79. Feng J, Hu X, Yue PL, Zhu HY, Lu GQ. Discoloration and mineralization of Reactive Red HE-3B by heterogeneous photo-Fenton reaction. Water research. 2003;37(15):3776-84.

80. Hanafi MF, Sapawe N. Effect of pH on the photocatalytic degradation of remazol brilliant blue dye using zirconia catalyst. Materials Today: Proceedings. 2020;31:260-2.

81. Akpan UG, Hameed BH. Parameters affecting the photocatalytic degradation of dyes using TiO_2-based photocatalysts: a review. Journal of hazardous materials. 2009;170(2-3):520-9.

82. Chakrabarti S, Dutta BK. Photocatalytic degradation of model textile dyes in wastewater using ZnO as semiconductor catalyst. Journal of hazardous materials. 2004;112(3):269-78.

83. Guo Q, Zhou C, Ma Z, Yang X. Fundamentals of TiO_2 photocatalysis: concepts, mechanisms, and challenges. Advanced Materials. 2019;31(50):1901997.

84. Di Paola A, Bellardita M, Palmisano L. Brookite, the least known TiO_2 photocatalyst. Catalysts. 2013;3(1):36-73.

85. Lettieri S, Pavone M, Fioravanti A, Santamaria Amato L, Maddalena P. Charge carrier processes and optical properties in TiO2 and TiO2-based heterojunction photocatalysts: A review. Materials. 2021;14(7):1645.

86. Padma C, Raja DH, Davidson DJ. Photodegradation of Methyl violet using Ag modified TiO2 nanotubes by UV and UV/H2O2. Chemical Physics Impact. 2023;7:100366.

87. Hussain M, Ceccarelli R, Marchisio D, Fino D, Russo N, Geobaldo F. Synthesis, characterization, and photocatalytic application of novel TiO_2 nanoparticles. Chemical Engineering Journal. 2010;157(1):45-51.

88. Primo A, Corma A, García H. Titania supported gold nanoparticles as photocatalyst. Physical Chemistry Chemical Physics. 2011;13(3):886-910.

89. Khan MI, Iqbal S, Nawaz M, Gohar S. Cr-Doped TiO_2: A Study on Optical and Photocatalytic Enhancement for Solar Wastewater Treatment. Available at SSRN 4935115. 2024.

90. Nguyen MD, Tran H-V, Xu S, Lee TR. Fe_3O_4 nanoparticles: structures, synthesis, magnetic properties, surface functionalization, and emerging applications. Applied Sciences. 2021;11(23):11301.

91. Liu S, Yu B, Wang S, Shen Y, Cong H. Preparation, surface functionalization and application of Fe_3O_4 magnetic nanoparticles. Advances in colloid and Interface Science. 2020;281:102165.

92. Hamed R, Sawalha S, Assali M, Shqair RA, Al-Qadi A, Hussein A, et al. Visible light-driven ZnO nanoparticles/carbon nanodots hybrid for broad-spectrum antimicrobial activity. Surfaces and Interfaces. 2023;38.

93. Maghsoudy-Louyeh S, Kropf M, Tittmann B. Review of progress in atomic force microscopy. The Open Neuroimaging Journal. 2018;12(1).

94. Bakatula EN, Richard D, Neculita CM, Zagury GJ. Determination of point of zero charge of natural organic materials. Environmental Science and Pollution Research. 2018;25:7823-33.

95. Si Y, Liu Y, Lai W, Ma Y, Shi J, Wang B, et al. A New Enthalpy of Formation Test Set Designed for Organic Fluorine Containing Compounds. Advanced Theory and Simulations. 2022;5(8):2200093.

96. Al-Salihi S, Bayati M, Jasim AM, Fidalgo MM, Xing Y. Magnetic mesoporous TiO_2/Fe_3O_4 nanocomposite adsorbent for removal of sulfamethazine from water. Environmental Advances. 2022;9:100283.

97. Cristiano E, Hu Y-J, Sigfried M, Kaplan D, Nitsche H. A comparison of point of zero charge measurement methodology. Clays and Clay Minerals. 2011;59(2):107-15.

98. Fathima K. Study on the Role of Gold Nanoparticles on External Beam Radiation Using Fricke Gel. Int J Innov Sci Res Technol. 2019;4:173-8.

99. Chrisnasari R, Ewing TA, Hilgers R, van Berkel WJ, Vincken J-P, Hennebelle M. Versatile ferrous oxidation–xylenol orange assay for high-throughput screening of lipoxygenase activity. Applied Microbiology and Biotechnology. 2024;108(1):266.

100. Atkins PW, De Paula J, Keeler J. Atkins' physical chemistry. 11th ed: Oxford university press; 2018.

101. El-Sabban HA, Hegazey RM, Hamdy A, Moustafa Y. Study on highly efficient Z-scheme pn heterojunction Fe_3O_4/N-Bi_2MoO6: Synthesis, characterization and visible-light-excited photocatalytic activity. Journal of Molecular Structure. 2022;1269:133755.

102. National Institute of Standards and Technology. Mass Spectrum of Acetic Acid 2024 [cited 2024 August 16, 2024]. Available from: https://webbook.nist.gov/cgi/cbook.cgi?ID=C64197&Mask=200#Mass-Spec.

103. National Institute of Standards and Technology. Mass Spectrum of Glycine 2024 [Available from: https://webbook.nist.gov/cgi/cbook.cgi?ID=C56406&Mask=200#Mass-Spec.

104. National Institute of Standards and Technology. Mass Spectrum of Methanol [Available from: https://webbook.nist.gov/cgi/cbook.cgi?ID=C67561&Mask=200.

105. Technology) NNIoSa. Mass Spectrum of Iminodiacetic acid [Available from: https://webbook.nist.gov/cgi/cbook.cgi?ID=C142734&Mask=200#Mass-Spec.

106. Badran I, Tighadouini S, Radi S, Zarrouk A, Warad I. Experimental and first-principles study of a new hydrazine derivative for DSSC applications. Journal of Molecular Structure. 2021;1229:129799.

107. Ruscic B. Active thermochemical tables: sequential bond dissociation enthalpies of methane, ethane, and methanol and the related thermochemistry. The Journal of Physical Chemistry A. 2015;119(28):7810-37.

108. Xue X-S, Ji P, Zhou B, Cheng J-P. The essential role of bond energetics in C–H activation/functionalization. Chemical reviews. 2017;117(13):8622-48.

109. Badran I, Hashlamoun K, Nassar NN. Bond dissociation energies of the fifth-row elements (In- I): A quantum theoretical benchmark study. International Journal of Quantum Chemistry. 2023;123(23):e27222.

Appendices

Appendix A

Figures

Figure 1

Schematic Representation of the Photocatalysis Mechanism

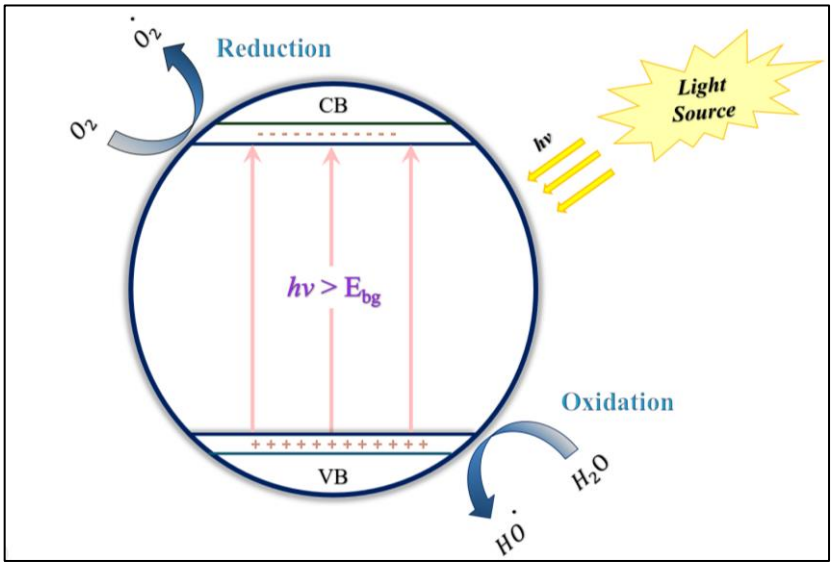

Figure 2

Photograph of the photocatalysis experimental set up.

Figure 3

Second day of treatment with catalyst under LED radiation

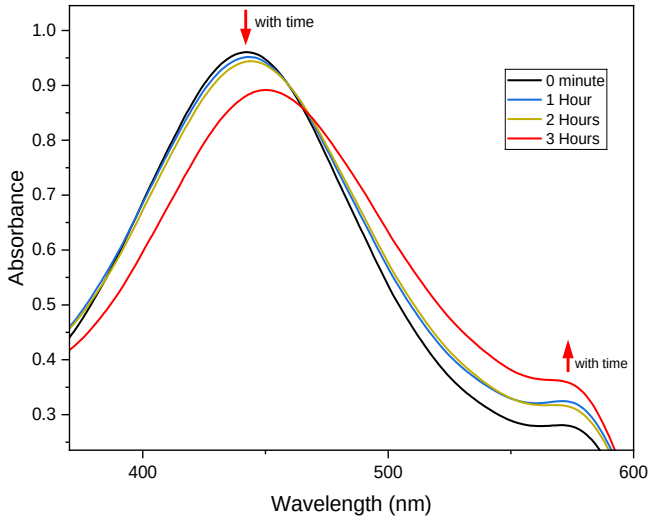

Figure 4

Third day of treatment with catalyst under LED radiation

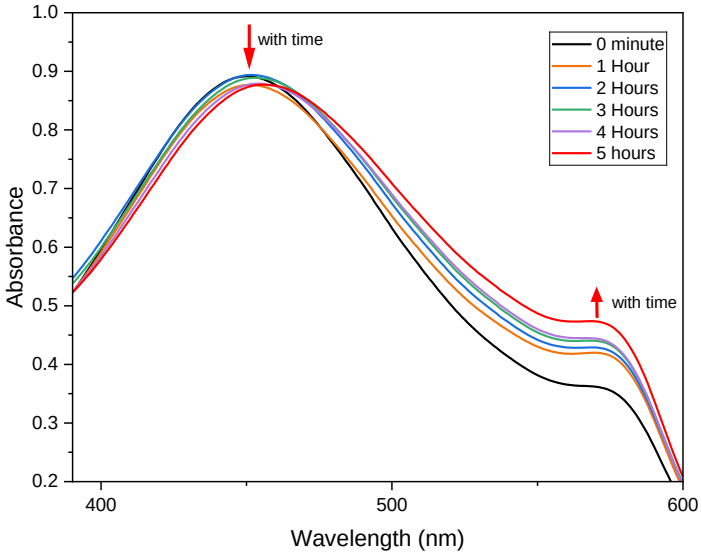

Figure 5

Second day of treatment with catalyst in the dark

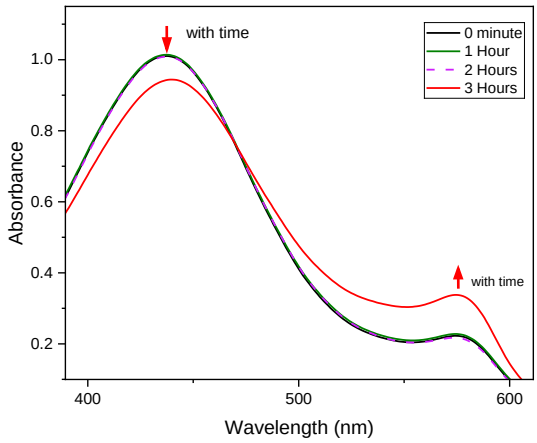

Figure 6

Third day of treatment with catalyst in the dark

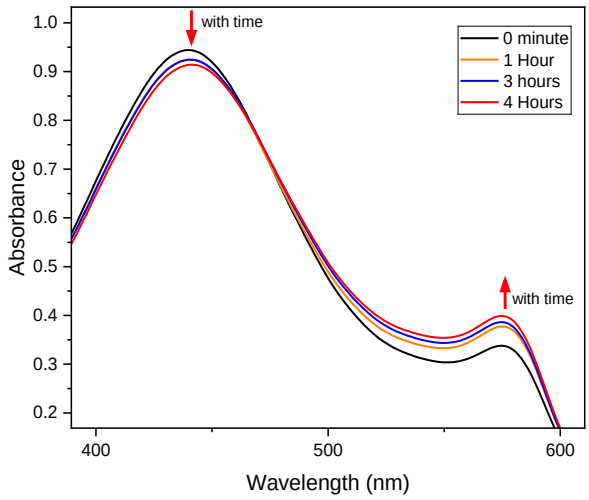

Figure 7

(a) first order plot of absorbance at 433 nm, (b) second order plot of absorbance at 433nm, (c) first order plot of absorbance at 578 nm,(d) second order plot of absorbance at 578 nm.

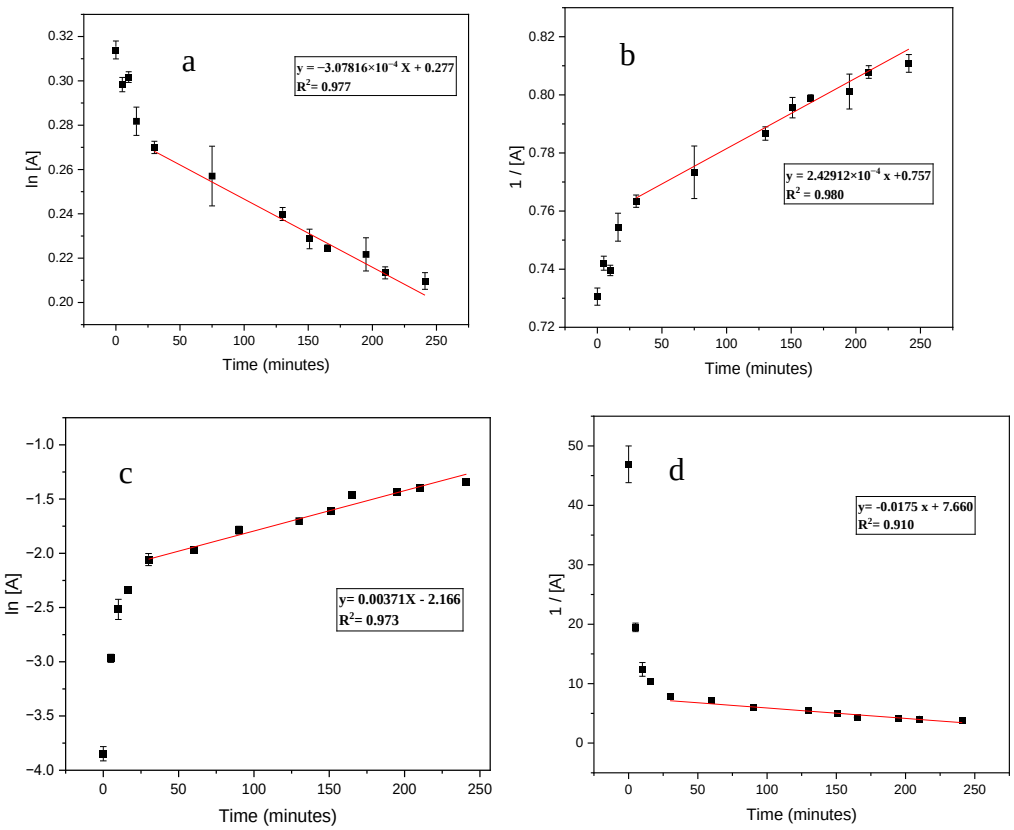

Figure 8

Percent change in absorption of Xylenol Orange with different amount of catalyst: (a) at 433 nm, (b) at 578 nm.

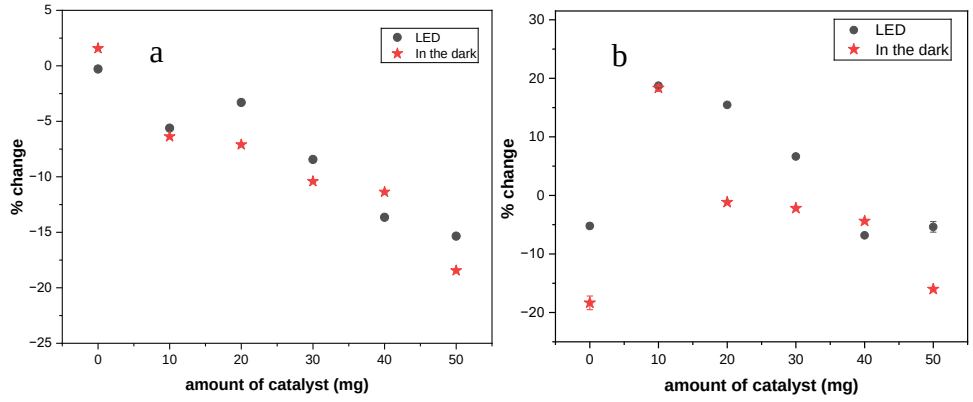

Figure 9

Percent change of absorption of Xylenol Orange with different concentrations at : (a) 433 nm, (b) 578 nm.

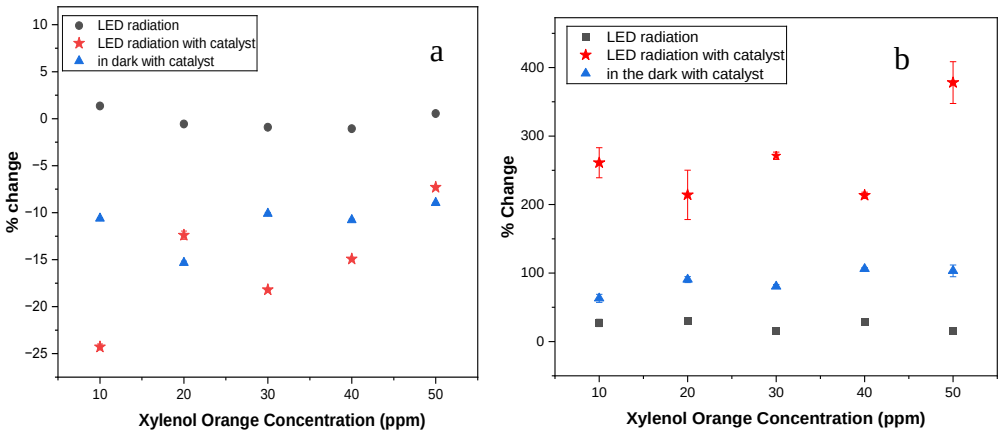

Figure 10

Mass spectra of acetic acid provided by :(a) GC mass detector for Xylenol Orange after photocatalysis treatment, (b) NIST webbook.

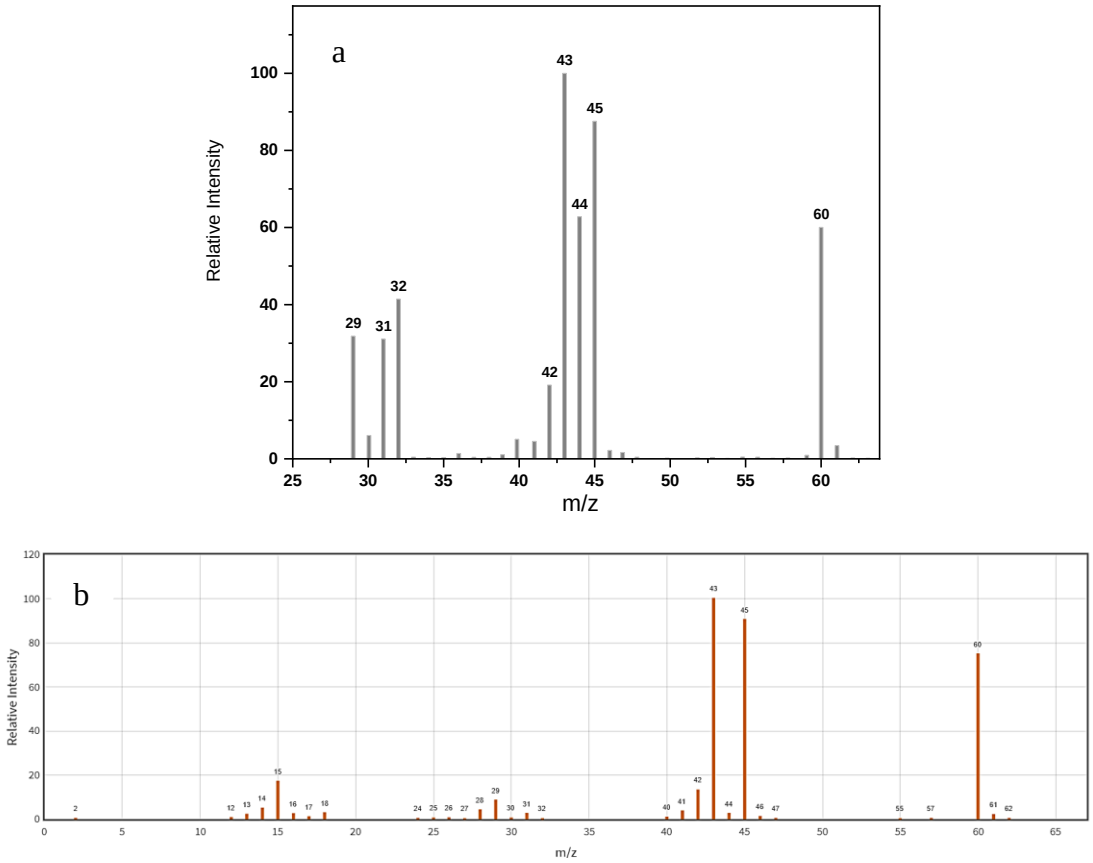

Figure 11

Mass spectra of :(a) intermediate formed at retention time of 2.062 mins of the treated Xylenol Orange, (b) Glycine from NIST, (c) methanol from NIST (d) iminodiacetic acid from NIST.

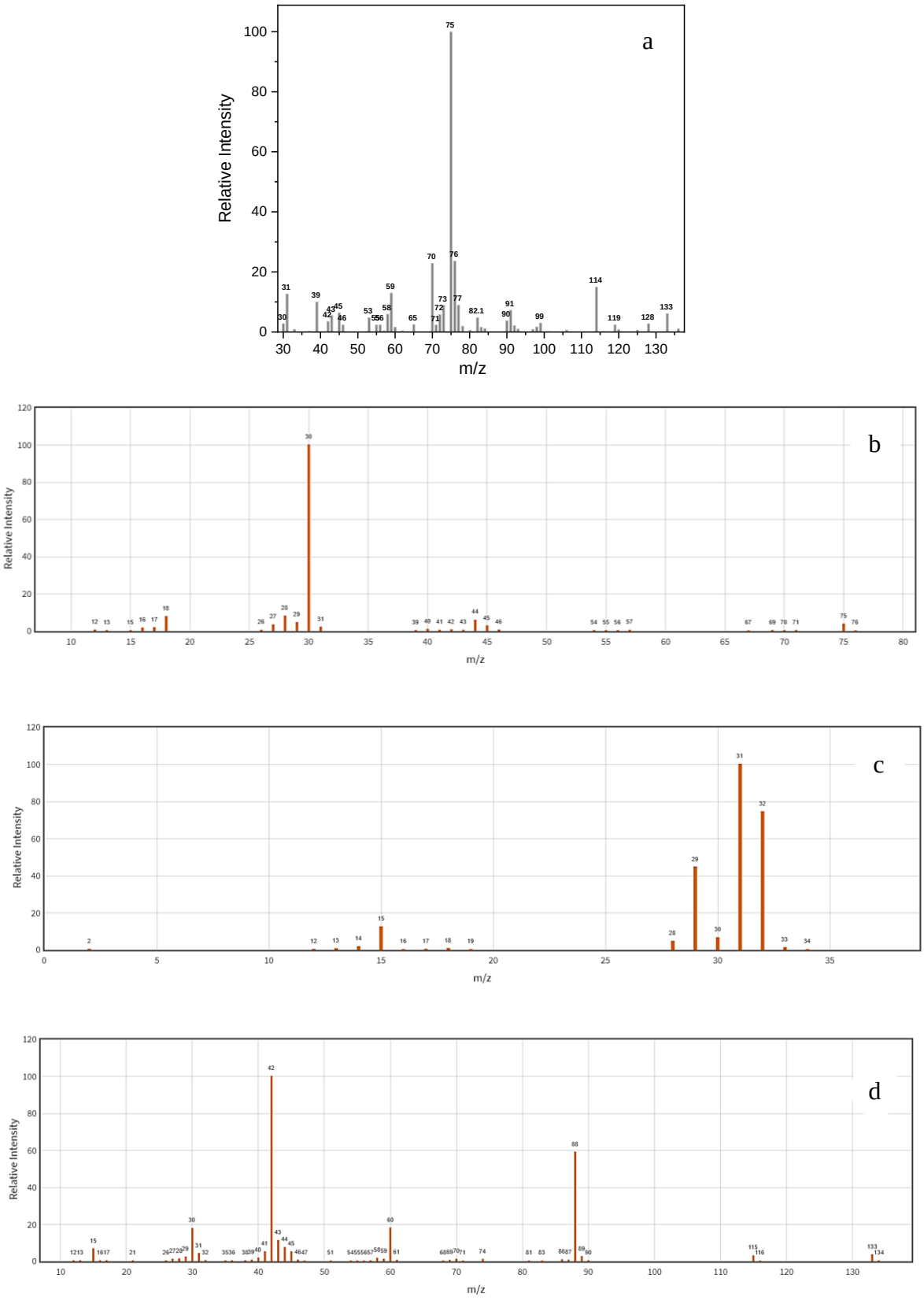

Figure 12

UV-Vis spectrum of Xylenol Orange sodium Salt in arbitrary unit obtained experimentally in the lab and by TD-DFT at B3LYP and ma-def2-SVP with CPCM (water) level of theory.

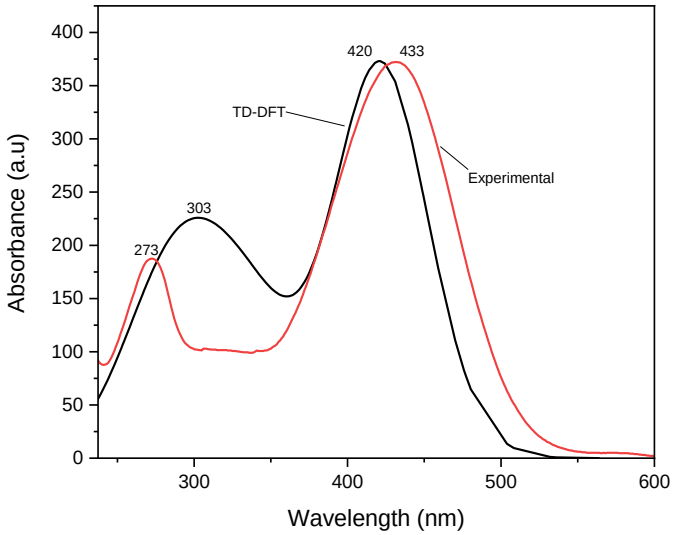

Figure 13

MO diagram of Xylenol Orange

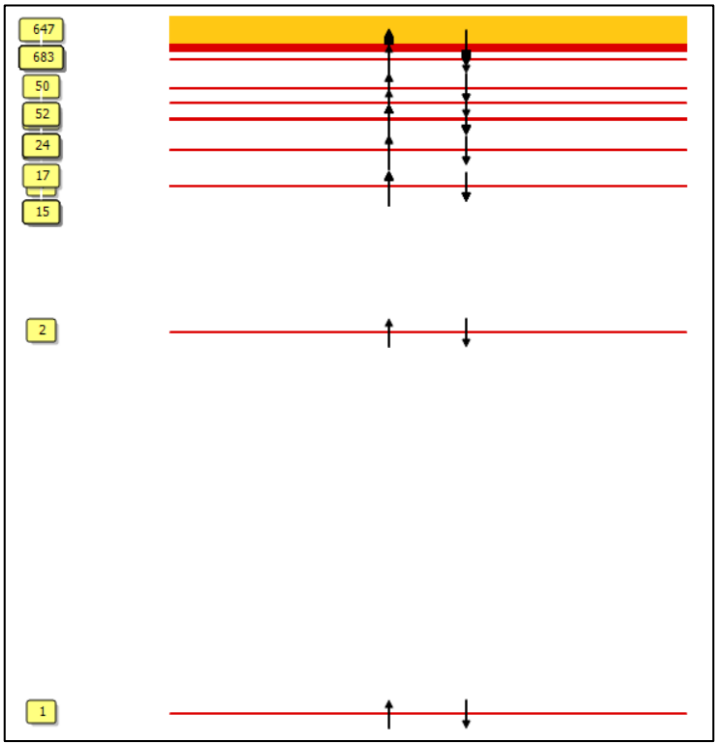

جـامعـــة النجاح الوطنية

كليـــة الدراســـات العليـــا

التحلل الضوئي لصبغة الزايلول البرتقالي باستخدام حفّاز مغناطيسي نانوي من $Fe_3O_4.TiO_2$ تحت تأثير الضوء المرئي

إعداد

نادين يوسف أحمد عباس

إشراف

د.إسماعيل بدران

د. روان خلف

قدمت هذه الرسالة استكمالا لمتطلبات الحصول على درجة الماجستير في الكيمياء، من كلية الدراسات العليا، في جامعة النجاح الوطنية، نابلس- فلسطين.

2024

التحلل الضوئي لصبغة الزايلول البرتقالي باستخدام حفّاز مغناطيسي نانوي من $Fe_3O_4.TiO_2$ تحت تأثير الضوء المرئي

إعداد

نادين يوسف أحمد عباس

إشراف

د.إسماعيل بدران

د. روان خلف

الملخص

الهدف من هذه الدراسة هو تطوير طريقة تحفيز ضوئي جديدة فعّالة واقتصادية لتنقية المياه من الأصباغ العضوية. تحقيق ذلك يتم من خلال عرض طريقة تصنيع حفّاز ضوئي جديد له فجوة طاقة صغيرة لجعله نشطًا تحت إشعاع الضوء المرئي (LED). هذا الحفّاز يمتلك خصائص مغناطيسية تجعل عملية تنقية المياه من الحفّاز بعد معالجتها أبسط . كما و تم في هذه الدراسة تصنيع الجسيمات النانوية المغناطيسية لـ $10\%TiO_2/Fe_3O_4$ وسط درجة حموضة قاعدية. كما و وجِدَ أن نقطة الشحنة الصفرية للحفّاز (PZC) تساوي 4.69. تم استخدام الجسيمات النانوية المغناطيسية كمحفز ضوئي لتنقية المياه من صبغة الزايلول البرتقالي العضوية تحت إشعاع الضوء المرئي (LED) .

أيضاً تم فحص خصائص التحفيز الضوئي للحفّاز السابق تحضيره تحت ظروف مختلفة. لوحظ أن الجسيمات النانوية المغناطيسية المصنعة لها نفس التأثير التحفيزي الضوئي التي تمتلكها جزئيات ثاني أكسيد التيتانيوم الروتيل. كما وتمت دراسة الظروف المختلفة المؤثرة على التحفيز الضوئي مثل: الوقت، ودرجة الحموضة للوسط، وتركيز صبغة الزايلول البرتقالي وكمية الحفّاز المستخدمة، وتأثير وجود وتركيز فوق أكسيد الهروجين. وقد لوحظ أن كفاءة التحفيز الضوئي لا تتأثر بتركيز محلول الزايلول البرتقالي وتنخفض مع زيادة كمية الحفّاز المستخدمة. كما وُجِد أنّ التحفيز الضوئي يُفضّل الظروف الحمضية بدرجة حموضة تساوي ~ 3، كما ويُفضّل وجود فوق أكسيد الهيدروجين. أيضاً أجريت دراسة حركية

للتفاعل، ووجد أن التحلل يزداد مع الوقت، وأن معدل سرعة التفاعل يتبع قوانين معدل تفاعل الرتبة الثاني. كما و تم فحص إمكانية إعادة استخدام الحفّاز مرة أخرى بعد المعالجة باستخدام عدة محاليل. وعليه وجد أن الإيثانول هو الحل الأمثل لمعالجة الجسيمات النانوية واستخلاصها بعد انتهاء عملية التحفيز الضوئي. كما واحتفظت الجسيمات النانوية بالخصائص المغناطيسية و قدرتها على التحفيز الضوئي بعد المعالجة. مما سبق، تم التأكيد على أنه يمكن استخدام الحفّاز الضوئي في أربع دورات على الأقل من التحفيز الضوئي. وفي الختام، يمكن استخدام الجسيمات النانوية المغناطيسية المصنعة من $10\%TiO_2/Fe_3O_4$ بكفاءة كمحفز ضوئي تحت تأثير أشعة الضوء المرئي (LED) لتنقية الملوثات العضوية ، مما يجعل الحفّاز اقتصادياً وصديقاً للبيئة.

كلمات مفتاحية

التحفيز الضوئي، التحلل الضوئي، الصمام الثنائي الباعث للضوء (LED)، الصبغة، الزايلول البرتقالي، الجسيمات النانوية، ثاني أكسيد التيتانيوم، مغناطيسي، Fe_3O_4، فوق أكسيد الهيروجين، الأشعة فوق البنفسجية المرئية، الطيف.